/CDF/ANAL/BOTTOM/CDFR/8705
v 2.00
April 9, 2007

Measurement of B^0 Branching Fractions Using Combined Mass and dE/dx Fits

Alessandro Cerri, Amanda Deisher, Hung-Chung Fang,
Johannes Mülmenstädt, Marjorie Shapiro
Ernest Orlando Lawrence Berkeley National Laboratory
Donatella Lucchesi, Simone Pagan Griso
University of Padova, I.N.F.N. — Padova
Giuseppe Salamanna
University of Rome "La Sapienza", I.N.F.N. — Rome

April 9, 2007

Abstract

Combined mass and dE/dx fits are used to measure the branching fractions in fully and partially reconstructed B decays in 1.2 fb^{-1} of data collected using the two-track trigger. The event selection and fitter are optimized for the measurement of the relative branching ratios $\mathcal{B}(B \to DK)/\mathcal{B}(B \to D\pi)$. We measure this ratio in the control samples $\overline{B}^0 \to D^+X$ and $\overline{B}^0 \to D^{*+}X$, obtaining $\mathcal{B}(\overline{B}^0 \to D^+K^-)/\mathcal{B}(\overline{B}^0 \to D^+\pi^-) = 0.092 \pm 0.005(\text{stat}) \pm 0.007(\text{sys})$ and $\mathcal{B}(\overline{B}^0 \to D^{*+}K^-)/\mathcal{B}(\overline{B}^0 \to D^{*+}\pi^-) = 0.084 \pm 0.008(\text{stat})$.

Contents

List of Figures

List of Tables

1 Introduction

Measurements of decays of the type $B \to DK$ provide important information on the CKM matrix. Cabibbo-suppressed B^+ decays can provide constraints on the angle γ using a variety of methods [1, 2, 3, 4, 5]. Time-dependent mixing measurements using the decay mode $B_s \to D_sK$ are expected in the long run to provide a measurement of γ that is theoretically very clean [6].

Such measurements require a robust fitting technique and event selection designed to minimize systematic uncertainties. This note describes an implementation of such tools and the application of the tools to two control samples ($B^0 \to D^{*-}K^+$ and $B^0 \to D^-K^+$). Two companion notes describe the treatment of the signal samples $B^+ \to \overline{D}^0K^+$ [7] and $B_s \to D_s^{\pm}K^{\mp}$ [8].

2 Reconstruction and Pre-Selection

This analysis uses the `B_CHARM` data samples `xbhd0d`, `xbhd0h` and `xbhd0i`, which together correspond to 1.2 fb^{-1}. The run range is 138809–222426. Hadronic decays of type $B \to D\pi$ were stripped using `CharmMods` and `cdfsoft` release 6.1.2. The `tcl` files, scripts and binary used for this strip can be obtained by creating a 6.1.2 offline test release and doing the following:

```
addpkg CharmMods Jan2006_BerkeleyStrip
addpkg BerkeleyB Jan2006_BerkeleyStrip
gmake CharmMods.nobin
gmake BerkeleyB.PrimeVtx
```

The `tcl` files used reconstruct the candidates are `BerkeleyB/macros/PrimeVtx/SK_driver_-start.tcl` and `BerkeleyB/macros/PrimeVtx/SKAll_frag_start.tcl`.

In the skim, tracks are refit using `TrackSelectorModule` and the B-group recommendations for the treatment of passive material using phantom layers, the rescaling of the COT covariance matrix and the rescaling of silicon-hit resolutions. L00 hits are included in the fit. Good tracks are required to have at least 2 axial and 2 stereo superlayers in the COT with at least 5 hits each and $|\eta| < 2.0$. Except for the soft pion used in D^{*+} reconstruction, tracks are required to have at least 3 silicon hits. Candidates are reconstructed in a variety of $B \to D\pi$ modes as follows:

- A D candidate is reconstructed using `D1VertModule` requiring at least one SVT-matched track. For the D^0 and D^+, the reconstructed mass is required to be between 1.81 and 1.92 GeV, while for the D_s the mass is required to be between 1.91 and 2.03 GeV. The D candidate is required to have a minimum L_{xy} of 200 μm.

- B candidates are formed by combining the D with another track (or two tracks for the D^*) and using `D2VertModule` to fit with `CTVMFT`. The invariant mass of the candidate is required to be between 4.65 and 6.5 GeV and the p_{T} is required to be > 5.5 GeV. An impact parameter cut $|d_0(B)| < 100$ μm is made on the B with respect to the beamline. Candidates are required to have $L_{xy} > 300$ μm and fit $\chi^2_{xy} < 30$. No mass constraint on the D is used for this selection.

- Candidates are required to have at least two tracks matched to SVT tracks (using the standard `CharmMods` association) and satisfying the `Scenario Low` requirements. Tighter trigger validation is performed during ntuple analysis.

- The event-by-event primary vertex is determined using the module `DCalcPrimVert-Module` with the default vertex scale factor of 1.38. No impact parameter or L_{xy} cuts are made based on kinematic quantities calculated using the event-by-event vertex in the skim.

Output from these skims has been stored in SAM. Table 1 lists the SAM datasets. Samples relevant for this note are `skbh24`, `skbh29` and `skbh30`.

Ntuples were created from these stripped samples using the `TagNt` package. The code and scripts used to create these ntuples can be built in an offline 6.1.2 test release by doing

```
addpkg TagNt run_12_13
```

and following the instructions in the file `TagNt/instructions.txt`. A brief description of the ntuple framework can be found in `TagNt/doc/guide.pdf`.

SAM Dataset	Decay Mode	
skbh13	$\overline{B}^0_s \to D^+_s\pi^-$	$(D_s \to K^*K)$
skbh14	$\overline{B}^0_s \to D^+_s\pi^+$	$(D_s \to K^*K)$
skbh16	$\overline{B}^0_s \to D^+_s\pi^-$	$(D_s \to 3\pi)$
skbh17	$\overline{B}^0_s \to D^+_s\pi^+$	$(D_s \to 3\pi)$
skbh21	$B^- \to D^0\pi^-,$	$(D^0 \to K\pi)$
skbh22	$B^- \to D^0\pi^-,$	$(D^0 \to \pi\pi)$
skbh23	$B^- \to D^0\pi^-,$	$(D^0 \to KK)$
skbh24	$\overline{B}^0 \to D^{*+}\pi^-$	$(D^{*+} \to D^0\pi,\ D^0 \to K\pi)$
skbh26	$\overline{B}^0_s \to D^+_s\pi^-$	$(D_s \to \phi\pi)$
skbh27	$\overline{B}^0_s \to D^+_s\pi^+$	$(D_s \to \phi\pi)$
skbh29	$\overline{B}^0 \to D^+\pi^-$	$(D^+ \to K^-\pi^+\pi^+)$
skbh30	$\overline{B}^0 \to D^+\pi^+$	$(D^+ \to K^-\pi^+\pi^+)$

Table 1: Skimmed datasets available in SAM

3 Selection of Candidates

The selection cuts used in this analysis are significantly tighter than those used in the baseline hadronic analyses for two reasons. First, because dE/dx is used to separate $B \to DK$ from $B \to D\pi(X)$ and background, the track coming from the B vertex (which for convenience we will call the B pion) is required to have the same momentum and track quality cuts as the tracks used to calibrate the dE/dx. Second, because we are interested in Cabibbo-suppressed modes, systematic uncertainties in modeling the background are more important than they are for the studies of Cabibbo-allowed decays. We therefore have chosen to tighten the kinematic cuts to further reduce the background.

3.1 $\overline{B}^0 \to D^{*+}X$ Cuts

The $\overline{B}^0 \to D^{*+}X$ cuts are identical to those optimized for the $B^- \to D^0X$; we will summarize the optimization procedure. Since the statistical uncertainty on $\mathcal{B}(B^- \to D^0K^-)/\mathcal{B}(B^- \to D^0\pi^-)$ is dominated by the statistical uncertainty on the $B^- \to D^0K^-$ yield, we attempt to maximize $S^2/(S+B)$ for the $B^- \to D^0K^-$ in as unbiased a way as possible. This method uses $B^- \to D^0X$ Monte Carlo for $B^- \to D^0K^-$, $B^- \to D^0\pi^-$, and the rest of $B^- \to D^0X$. The combinatorial background is taken from the high sideband of the statistically independent $\overline{B}^0 \to D^+X$ sample. After scaling the $B^- \to D^0X$ Monte Carlo and D^+X data yields to that expected in D^0X data and taking into account the shape of the combinatorial background, the cuts are scanned and $S^2/(S+B)$ calculated for each combination of cuts. The signal S is the $B^- \to D^0K^-$ yield, whereas the background B includes $B^- \to D^0\pi^-$, the rest of

$B^- \to D^0X$, and the combinatorial background.

We have looked at 18 variables with varying degrees of correlations amongst themselves. We chose seven variables that are relatively uncorrelated and show reasonable potential for the purpose of separating signal from background. Three of these (iso(B), $z_0(B)$, and $d_0(B)$ significance) are not modeled by `Bgenerator` Monte Carlo; we fix these cuts at values that keep most of the signal. The remaining four variables are then subject to a four-dimensional optimization using the method explained above. These four variables are simultaneously scanned in the following ranges:

- $L_{xy}(B)$ significance: 9 steps in the range 4 to 12
- $p_{\mathrm{T}}(\pi_B)$: 5 steps in the range 2 to 3 GeV
- $L_{xy}(B \leftarrow D)$ significance: 9 steps in the range -6 to 2
- B vertex probability: 4 steps in the range 10^{-6} to 10^{-3}

$S^2/(S+B)$ and its error are calculated for each of the 1620 scan points. The results are sorted by $S^2/(S+B)$. Many of the $S^2/(S+B)$ points are statistically indistinguishable. Out of the top few dozen in $S^2/(S+B)$, as our optimal point, we pick a cut combination that does not put us in a strange corner of cut space.

3.2 $\overline{B}^0 \to D^+X$ Cuts

For the $\overline{B}^0 \to D^+X$ selection, we use the mixing analysis rectangular cuts [9] as a starting point. The p_{T} of the B pion from the has to be larger than 2 GeV in order to use dE/dx. We also choose to veto D^+ candidates consistent with $D^{*+} \to D^0(K^-\pi^+\pi^0)\pi^+$ and $\Lambda_c \to pK^-\pi^+$ instead of including their templates in the mass fit. By performing one-dimensional $S^2/(S+B)$ optimizations of the remaining cut variables, we arrived at the following changes in cuts:

- $|d_0(B)|$ from 110 μm to 60 μm
- $L_{xy}(B \leftarrow D)$ from -300 μm to 0
- $\chi^2_{xy}(B)$ from 15 to 10

We also loosen the $L_{xy}(B)$ significance cut from 11 to 8. For the optimization, S and B were taken from the B peak region (5.26 GeV $< m(B) <$ 5.4 GeV). The D sidebands were used as the background and the sideband-subtracted D peak events were used as signal.

Since the combinatorial background is a large source of systematic uncertainty, we apply the z_0B and isolation cut from the B^+ optimization for further background reduction.

3.3 Cut variables

A complete set of analysis cuts for each decay mode is presented in Table 2. When cutting on χ^2_{xy} probability, we rescale χ^2_{xy} by 1/1.7; this procedure is based on a study which showed that a scale factor of 1/1.7 yields a flat probability distribution. The variable $z_0(B)$ is the impact parameter of the B candidate with respect to the three-dimensional event-by-event primary vertex. The isolation of the B candidate iso(B) ($\Delta R < 1$) is defined as

$$\mathrm{iso}(B)\ (\Delta R < 1) = \frac{p_{\mathrm{T}}(B)}{p_{\mathrm{T}}(B) + \sum\limits_{\mathrm{tracks}} p_{\mathrm{T}}(\mathrm{track})} \tag{3·1}$$

where the sum extends over tracks within $\Delta R < 1$ of the B.[1] The SVT match distance is calculated in ϕ_0 and curvature. To veto the reflection of Λ_c into the D^+ mass peak, we calculate $m(K, \pi \mapsto p, \pi)$, the mass of a D^+ candidate reconstructed as a Λ_c by reassigning one of the pion tracks to a proton hypothesis. The veto applies if reassigning either of the two pions places the candidate in the Λ_c mass window. We veto the decay $D^{*+} \to D^0(K^-\pi^+\pi^0)\pi^+$ reconstructed as $D^+ \to K^-\pi^+\pi^+$ by calculating $m(K\pi\pi) - m(K\pi)$. The veto applies if either combination of pions yields $\Delta m < 180$ MeV. Z is the PID variable defined in (5·1). We calculate Z using the macro provided by Stefano Giagu [10] as described in Section 5.2. If the macro signals an invalid dE/dx measurement by returning $Z = -999$, the candidate is discarded.

The mass distributions for the candidates with these selections are shown in Figures 1–2.

4 Monte Carlo Samples

Monte Carlo samples for $B \to DX$ modes have been generated using `Bgenerator` and `EvtGen` in offline release 5.3.4. Detector and trigger simulation are performed using standard B group recommendations. A description of the samples, along with all relevant scripts and `tcl` files, is available in [11]. A list of relevant samples is given in Table 3. Figures 3–6 show the composition of the samples used for the D^+ fit; Figures 7–9 show the composition of the samples used for the D^{*+} fit.

Monte Carlo samples are reconstructed using the same `tcl` scripts that are used for data, with one trivial exception. The default magnetic field in the B group Monte Carlo scripts is set to 1.4116 T rather than the value of 1.41296 T that is appropriate for real data, so the B field specified in the reconstruction `tcl` files has been appropriately modified. It should be noted that even with this correction to the B field the reconstructed D and B masses in the Monte Carlo samples differ slightly from those in data. An overall scale factor of

[1] Since the Monte Carlo samples are produced with `Bgenerator`, the isolation cut has no effect on Monte Carlo.

	$B^0 \to D^-(K^+\pi^-\pi^-)\pi^+$	$B^0 \to D^{*-}\left(\overline{D}^0(K^+\pi^-)\pi^-\right)\pi^+$
$\chi^2_{xy}(B)$	< 10	
$\mathrm{prob}(\chi^2_{xy}(B)/1.7, n(\mathrm{dof}))$		> 0.001
$\chi^2_{xy}(D)$	< 15	
$L_{xy}(B)/\sigma_{L_{xy}}(B)$	> 8	> 8
$L_{xy}(B \leftarrow D)$	> 0	
$L_{xy}(B \leftarrow D)/\sigma_{L_{xy}}(B \leftarrow D)$		> -2
$\lvert d_0(B)\rvert$	$< 60\ \mu$m	
$\lvert d_0(B)/\sigma_{d_0}(B)\rvert$		< 3
$p_{\mathrm{T}}(B)$	> 5.5 GeV	
$p_{\mathrm{T}}(\pi_B)$	> 2.0 GeV	> 2.0 GeV
$\Delta R(D, \pi_B)$	< 1.5	
$\lvert z_0(B)/\sigma_{z_0}(B)\rvert$	< 3	< 3
$\mathrm{iso}(B)$ ($\Delta R < 1$)	> 0.5	> 0.5
$m(D^+)$	$\lvert m/\mathrm{MeV} - 1869.4\rvert < 20$	
$m(D^0)$		$\lvert m/\mathrm{MeV} - 1864.6\rvert < 20$
$m(D^{*+}) - m(D^0)$		$144 < \Delta m/\mathrm{MeV} < 147$
π_B SVT match distance	< 25	< 25
π_B SVT χ^2	< 15	< 15
π_B SVT p_{T}	> 2 GeV	> 2 GeV
$m(K, \pi \mapsto p, \pi)$	$\lvert m/\mathrm{MeV} - 2285\rvert > 250$	
$m(K\pi\pi) - m(K\pi)$	$\Delta m/\mathrm{MeV} > 180$	
Z	$\neq -999$	$\neq -999$
Good run list	B_s mixing version 14	B_s mixing version 14

Table 2: Final cuts used to select candidates for this analysis. See the text for an explanation of the more esoteric cut variables.

Channels			Sample name
	$\overline{B}^0 \to D^+\pi^-$ fit		
$\overline{B}^0$	$\to$	$D^+\pi^-(n\gamma)$	b0dkpp
$\overline{B}^0/B^0$	$\to$	D^+X	z35ba0
B^-/B^+	$\to$	D^+X	bdpkpx
B_s	$\to$	$D_s^-(\phi\pi^-)X$	mcbh03
	$\overline{B}^0 \to D^{*+}\pi^-$ fit		
$\overline{B}^0$	$\to$	$D^{*+}\pi^-(n\gamma)$	b0dspp
$\overline{B}^0/B^0$	$\to$	$D^0\pi^+X$	z35b90
B^-/B^+	$\to$	$D^0\pi^+X$	bd0kpx

Table 3: Monte Carlo samples used in this analysis. The samples are available in SAM or in the process of being copied to SAM.

1.00025 ± 0.00012 is therefore applied to all Monte Carlo mass distributions. In addition, the mass resolution in the Monte Carlo is slightly better than in the data. Looking at the clean $\overline{B}^0 \to D^{*+}\pi^-$ sample, we find that Monte Carlo mass distributions agree with data if the Monte Carlo data is convoluted with a gaussian resolution function of width 6.43 ± 2.09 MeV. In Section 6.5 we assign a systematic uncertainty on the measured branching ratios by varying the smearing and scaling within their errors.

5 Fit Methodology

Data are fit using an unbinned extended or non-extended maximum likelihood fit. The fit variables are the invariant mass m of the candidate in the $D\pi$ mass hypothesis and the PID variable

$$Z = \log\left(\frac{dE/dx(\text{measured})}{dE/dx(\text{expected for } \pi)}\right) \tag{5·1}$$

for the B daughter track. The likelihood function is

$$L(\mu_1, \ldots, \mu_M) = \frac{\exp(-\sum_j \mu_j)}{N!} \prod_{i=1}^{N} \sum_{j=1}^{M} \mu_j \, p_j(m_i) \, q_j(Z_i) \tag{5·2}$$

in the extended case and

$$L(f_1, \ldots, f_{M-1}) = \prod_{i=1}^{N} \sum_{j=1}^{M} f_j \, p_j(m_i) \, q_j(Z_i), \quad \text{where } f_M = 1 - \sum_{j=1}^{M-1} f_j \tag{5·3}$$

in the non-extended case. $\prod_i$ is a product over all N candidates and $\sum_j$ is a sum over the M components (decay modes and background) of the fit. In the extended fit, μ_j is the number of candidates in the j-th component; in the non-extended, f_j is fraction of candidates in the j-th component. The number of independent parameters is one smaller in the non-extended fit than in the extended fit, since the normalization of the last component is fixed by the normalization of the other components. The mass pdf's $p_j(m)$ and Z pdf's $q_j(Z)$ (also referred to as dE/dx pdf's) are described in greater detail below.

Various additional features are supported. We summarize them here and describe them in greater detail when we make use of them.

- Gaussian constraints on the ratios between components can be imposed to reflect PDG values of known branching fractions.

- A component can be set to a fixed fraction of another component. This feature is useful in the treatment of the $q(Z)$ of the B-physics background.

- Parameters beyond the $\mu_1, \ldots, \mu_M$ can be used; shape parameters for the background mass pdf's are an example.

- Z templates can be broken up into multiple mass regions.

- Parameters can be fixed.

The choice of fit components is channel-dependent. In all cases, these components can be characterized as coming from one of three possible sources:

- D plus track combinations where the D and the track come from a single B hadron. We will call the pdf's from such samples "single-B templates". The mass pdf's for these components are determined from the Monte Carlo samples described in Section 4. Because we know for each Monte Carlo sample the species of the track that is combined with the D, the dE/dx pdf's are known. In general the fits have several components of this type (see Subsection 5.1 below).

- Cases where the D candidate does not come from a real D. We will call the pdf's for this case "fake-D templates." Both the mass and dE/dx pdf's for this component are measured in the data using the D sidebands. The normalization of this fit component can be determined by extrapolating the fake-D rate into the D signal region. This is not done in the default fit configuration, but it is used in a systematics study.

- D plus track combinations where a real D is combined with a track coming from fragmentation, the underlying event or the other B. We will call the pdf's from such samples "real-D background templates". The mass and dE/dx templates for this component are taken from the wrong-sign (*e.g.*, $B^0 \to D^- \pi^-$) data.

5.1 Mass Templates

The single-B templates are divided into several components corresponding to different decay modes. One place where special care has been taken is in the treatment of the radiative tail in the Cabibbo-allowed decay $B \to D\pi$. This radiative tail is important for two reasons. First, proper treatment of the tail is important for properly determining the number of events in the Cabibbo-allowed mode. Second, this tail puts additional $D\pi$ events into the region of the Cabibbo-suppressed decay $B \to DK$. The radiative tail on the Cabibbo-allowed mode is modeled in `EvtGen` by using `PHOTOS`. This model is expected to describe the shape of the tail well, but its reliability for determining the rate is not known. We therefore choose to leave the size of the radiative tail as a free parameter in our fit. Monte Carlo events in the Cabibbo-allowed mode are separated into a non-radiative subsample and a radiative one, and separate mass templates are created for each subsample. The `PHOTOS` cut-off in `EvtGen` is left at the default 10 MeV.

Figures 10 and 11 show the mass templates used in the D^+ and D^{*+} fits. It is clear that some of the templates are not easily described by a simple parametric shape. Since our Monte Carlo statistics are larger by at least a factor 3 than those of our data, we therefore choose to represent the mass pdf's for the single-B fit components as histograms. As noted above, the mass resolution in Monte Carlo is slightly better than in the data. We therefore re-smear the mass histograms obtained from the Monte Carlo by convolving them with a gaussian of width 6.43 MeV. Our original skim had a minimum mass cut of 4.65 GeV. After this convolution, we limit our mass fit range to above 4.85 GeV in order to avoid edge effects from the smearing. This mass cut also limits our sensitivity to a mass region in which the B branching fractions are poorly known.

In contrast, the statistics for the fake-D templates are limited (the maximum size of the sideband is determined by the D mass range included in the original skim). This situation is further complicated by the fact that poorly reconstructed real D's (which we assume below to come from $B \to DX$) also populate the sideband region. We therefore choose to describe the fake-D mass template using a smooth function:

$$p_{\rm bg}(m) = \frac{\alpha(1-\beta)\exp(-\alpha m)}{\exp(-\alpha m_{\rm min}) - \exp(-\alpha m_{\rm max})} + \frac{\beta}{m_{\rm max} - m_{\rm min}} \qquad (5{\cdot}4)$$

where $m_{\rm min}$ and $m_{\rm max}$ are the limits of the fit range. The parameters of the function are determined by fitting the $D\pi$ mass distribution for events in the D sideband to a fake-D component of the form (5·4) and a "poorly measured real-D" component, *i.e.* real D candidates far in the tails of the mass distribution. The shape (but not the normalization) of the real-D part of this fit is a histogram taken from the D sidebands in Monte Carlo. It is possible to determine the normalization of the fake-D component by fitting for the size of the combinatorial background under the D mass peak; this fit is described in detail in Section 6.1.2.

The real-D combinatorial background is modeled using the wrong-sign data. We plot the invariant mass of the wrong-sign candidates in the $D\pi$ mass assumption and sideband-subtract in the D mass. Then we perform a binned fit of this background-subtracted mass plot using a function of the form (5·4). In all samples, the rate of real-D combinatorial background is smaller than the fake-D. For example, in the $D^+\pi^-$ sample, only about 30% of the rate in the region above 5.4 GeV comes from real D^+.

5.2 Z Templates

As noted above, we choose to fit in Z, the logarithm of the ratio of the measured dE/dx to the predicted dE/dx for a pion. This variable is expected to have a more gaussian pdf than the dE/dx itself, which follows a log-normal distribution.

We determine the Z templates for pions and kaons from prompt D^{*+} data. This procedure is described in detail in a dedicated note [12]. The flavor of the daughter tracks of the D^0 in the decay $D^{*+} \to D^0(K^-\pi^+)\pi^+$ is tagged by the charge of the pion from the D^{*+}. Taken together with the large signal-to-background ratio of the Δm peak, this yields a very clean sample of pions and kaons. In addition, we sideband-subtract in Δm. To be used in the templates, the D^0 daughters are required to have $p_{\mathrm{T}} > 2$ GeV and to be SVT tracks. The Z calculated for the track uses the macro provided for this purpose [10] and therefore includes all the corrections described in [13]. In addition, we apply a correction based on run number, which is described in [12]. Templates are derived separately for `xbhd0d`, `xbhd0h` and `xbhd0i`. For the combined fit, we combine the separately derived templates.

We correct for two additional effects. The first effect is a momentum dependence of the Z of kaon tracks even after correction, which persists since the corrections are performed under an incorrect mass hypothesis. The detailed description of the second effect is the subject of [12]. Briefly, the measured dE/dx of a track depends on the tracking chamber activity in the vicinity of the track. It is therefore necessary to reweight the templates to account for higher activity in the template samples. Several variables are useful proxies for the chamber activity. The default variable is the track *secance*, or number of r–ϕ intersections with other tracks between the COT inner and outer radius. We choose this variable because it results in the best agreement between templates derived from non-prompt and prompt D^* decays. One of the other plausible proxy variables, the total number of tracks in the event, is considered in a systematics study (Section 6.5).

Because the $B \to DX$ templates contain semileptonic decays, we need to parameterize the dE/dx response for muons and electrons. For muons, we use the same templates as for pions. (Because these semileptonic components are small in the mass region of interest, systematic uncertainties associated with this choice are negligible.) For electrons, we generate a template from Monte Carlo using the predicted values of the electron dE/dx and its resolution from [13].

The Z templates for the combinatorial backgrounds are taken directly from the data.

Details vary between samples; a more detailed description can be found in Sections 6 and 7.

6 $\overline{B}^0 \to D^+\pi^-$ Fit

In this section we apply the fit to the $\overline{B}^0 \to D^+\pi^-$ sample. We describe the fit configuration, the systematic uncertainties and the fit results.

6.1 Configuration

The fit is an extended unbinned maximum-likelihood fit. The $D\pi$ mass does not use a mass constraint on the D candidate. (This requirement stems from our modeling of the fake-D background; see below.) Table 4 lists the fit components.

6.1.1 Single-B templates

The mass templates marked "Monte Carlo" are selected from single-B Monte Carlo according to the decay channels shown in Table 4. The Monte-Carlo candidate subsets used in the single-B templates are disjoint; the templates are listed in order of precedence. With a few exceptions, the partially reconstructed modes are collected in the "remainder" $\overline{B}^0/B^- \to D^+X$ template. $D^+\rho^-$ and $D^{*+}\pi^-$ are split out because these components leak into the D^+K^- mass region. The branching ratio $\mathcal{B}(B^- \to D_2^*\pi^-)$ used in our Monte Carlo generation was estimated based on an upper limit. The branching ratio has since been measured [14]. The $D^{(*)}K^{(*)}$ modes are the largest group of modes in which the track recoiling against the D^+ is a kaon; we split this group from the remainder template so we can give it a kaon dE/dx template. Likewise, we split out the $D^+e^\pm X$ decays and give them an electron dE/dx template. The $D^{(*)}K^{(*)}$ and $D^+e^\pm X$ components that are "split out" of the remainder template do not have floating normalizations but are instead fixed to the remainder template with ratios determined from the Monte Carlo. Lastly, a $B_s \to D_s^-(\phi\pi^-)X$ template is also included in the fit. The "parameter" column of the table summarizes the connections between the various templates.

6.1.2 Fake-D templates

The fake-D mass template is obtained as follows. The invariant mass under the $D^+\pi^-$ mass assumption is calculated in the sidebands of the D mass: 1.825 GeV $< m(D^+) <$ 1.84 GeV or 1.9 GeV $< m(D^+) <$ 1.915 GeV. This data is used in an unbinned mass-only fit with two components. The first component is a function of the form (5·4). The second component is a histogram obtained from the $B^0 \to D^-X$ MC (`z35ba0`) selecting on the D sideband. Figures 14–17 show the results of this fit in the three data samples. The shape parameters obtained from this auxiliary fit are fixed in the $\overline{B}^0 \to D^+\pi^-$ fit. Because the Monte-Carlo modeling of B candidates is less accurate in the tails of the D mass distribution than in the center, we find that the fake-D fits must be performed on candidates that are not mass-constrained. Therefore we use unconstrained candidates for all fit components.

It is possible to determine the normalization of the fake-D component before fitting. To do this, we fit the D mass plot with two gaussians (for the D signal) and a linear background. (This fit is binned.) These fits are shown in Figures 18–21. In the default $\overline{B}^0 \to D^+\pi^-$ fit, this constraint on the fake-D normalization is not used; it is used in one of the systematics studies.

6.1.3 Real-D templates

The real-D template is obtained from a binned fit of the $D\pi$ mass of wrong-sign candidates selected with the same cuts as the right-sign candidates but sideband-subtracted in the D mass. The fit function is of the form (5·4). These fits are shown in Figures 22–25. The shape parameters obtained from this auxiliary fit are fixed in the $\overline{B}^0 \to D^+\pi^-$ fit; the normalization is floating.

6.1.4 Z templates

The Z templates marked "prompt D^*" are described in Section 5.2 and in [12]. The effects treated in [13] and a residual time dependence are corrected for. Two-dimensional reweighting in secance (s) and momentum (p) is applied. The DeX template uses the parametric dE/dx simulation described in Section 5.2. The D_sX template is composed from e, μ (using π as proxy), π and K templates according to species fractions determined from the $B_s \to D_sX$ Monte-Carlo sample. The D_sX Z template is divided into four mass regions: the region below the D^+K^- (4.85 GeV $< m(B) <$ 5.17 GeV); the D^+K^- region (5.17 GeV $< m(B) <$ 5.26 GeV); the $D^+\pi^-$ region (5.26 GeV $< m(B) <$ 5.4 GeV); and the region above the $D^+\pi^-$ (5.4 GeV $< m(B) <$ 6.45 GeV).

The Z template for the fake-D component is taken directly from the D sideband data. The Z template for the real-D component is taken from the wrong-sign D data, selecting on the D peak. We divide both combinatorial-background templates into two B-mass regions (4.85 GeV $< m(B) <$ 5.4 GeV and 5.4 GeV $< m(B) <$ 6.45 GeV) to account for their B-mass dependence. (A study has been performed to show that the choice of two regions instead of four has no effect on the fit result.) In addition, signal subtraction is performed on the fake-D template to account for the leakage of poorly measured real D into the D sidebands. Because of limited statistics, sideband subtraction is not performed on the real-D Z template.

6.2 Results

Results of the likelihood fit are given in Table 5. Mass projections are shown in Figures 26–29. Z projections are shown in Figures 34–37. The four mass regions used in the Z projections are the same as described above for the D_sX template. Figure 42 shows the likelihood profiles in all fit parameters.

To calculate ratios of branching fractions from ratios of fit fractions, we proceed as follows. Let μ_1 and μ_2 be the normalizations of the fit components whose ratio of branching ratios $\mathcal{B}_1/\mathcal{B}_2$ we want to measure. The relationship between these quantities is

$$\frac{\mathcal{B}_1}{\mathcal{B}_2} = \frac{\mu_1/(\varepsilon_1\phi_1\eta_1)}{\mu_2/(\varepsilon_2\phi_2\eta_2)}, \tag{6·1}$$

where ε_i is the kinematic efficiency for a channel i, ϕ_i is the fraction of candidates in the fit mass range and η_i is the efficiency for the track species recoiling against the D in channel i to trigger.

ε_i and ϕ_i can be determined from MC: the MC yield y_i of a channel is related to the number N of candidates generated and the branching fraction $\mathcal{B}'_i$ used in the generator by

$$y_i = N\mathcal{B}'_i\varepsilon_i\phi_i. \tag{6·2}$$

Therefore, the relationship between the fit fractions and the ratio of branching ratios is

$$\frac{\mathcal{B}_1}{\mathcal{B}_2} = \frac{\mu_1\mathcal{B}'_1/(y_1\eta_1)}{\mu_2\mathcal{B}'_2/(y_2\eta_2)} \tag{6·3}$$

as long as the two channels are created in the same MC generation.

The relative trigger efficiency η_K/η_π between K and π tracks is determined in Sec. 14 of [15]. In detail, we use the XFT efficiency function provided by Stefano Giagu, which returns a weight $w(p_{\mathrm{T}}|\text{species})$ depending on run-number, p_{T} and track species as well as a $\pm 1\sigma$ systematic $\varsigma(p_{\mathrm{T}}|\text{species})$, as follows:

$$\begin{gathered}
\langle w_{DK}\rangle = \tfrac{1}{n_{DK}}\sum_{i\in K} w(p_{\mathrm{T}}^i|K), \quad \langle w_{DK}^2\rangle = \tfrac{1}{n_{DK}}\sum_{i\in K} w^2(p_{\mathrm{T}}^i|K) \\
\left\langle w_{DK}^{\pm}\right\rangle = \tfrac{1}{n_{DK}}\sum_{i\in K} w(p_{\mathrm{T}}^i|K) \pm \varsigma(p_{\mathrm{T}}^i|K) \\
\sigma_{DK} = \sqrt{\langle w_{DK}^2\rangle - \langle w_{DK}\rangle^2}/\sqrt{n_{DK}}, \quad \varsigma_{DK}^{\pm} = \left\langle w_{DK}^{\pm}\right\rangle - \langle w_{DK}\rangle
\end{gathered} \tag{6·4}$$

and

$$\begin{gathered}
\langle w_{D\pi}\rangle = \tfrac{1}{n_{D\pi}}\sum_{i\in \pi} w(p_{\mathrm{T}}^i|\pi), \quad \langle w_{D\pi}^2\rangle = \tfrac{1}{n_{D\pi}}\sum_{i\in \pi} w^2(p_{\mathrm{T}}^i|\pi) \\
\sigma_{D\pi} = \sqrt{\langle w_{D\pi}^2\rangle - \langle w_{D\pi}\rangle^2}/\sqrt{n_{D\pi}}
\end{gathered} \tag{6·5}$$

The summations run over candidates in the $\overline{B}^0 \to D^+X$ Monte-Carlo sample with a track of the indicated species recoiling against the D^+. The systematic error ς due to the XFT efficiency is calculated only for DK because ς_{DK} and $\varsigma_{D\pi}$ are correlated. We determine a correction factor $\eta_\pi/\eta_K = \langle w_{D\pi}\rangle / \langle w_{DK}\rangle = 1.0499 \pm 0.0281$. The error is calculated by propagating $\sigma_{D\pi}$, σ_{DK} and $\varsigma^{\pm}_{DK}$. Table 7 shows the corrected branching fractions. We calculate the errors taking into account the off-diagonal terms of the error matrix.

6.3 Fitter Validation

We validate the fitter by plotting the pull distributions of the fit parameters. Data is generated by throwing dice against the mass and dE/dx templates with the μ_j determined in the fit as the "true" μ_j, yielding a generated number of candidates that is Poisson-distributed about μ_j. The data is then fit. Figure 43 shows that the fit provides unbiased results and that the error estimate is correct. Table 8 lists the pull means and widths for 10000 pseudoexperiments of 46498 events each.

6.4 Studies of the Z Residual Bump

One discrepancy between the data and the fit model remains. The Z residual plot in the mass region dominated by $D^+\pi^-$ (5.26 GeV $< m(B) <$ 5.4 GeV) shows an excess between $Z = -0.2$ and $Z = -0.1$. We first perform a kaon projection of the mass plot, where each candidate is given a weight

$$w(Z) = \frac{Z - \langle Z(\pi)\rangle}{\langle Z(K)\rangle - \langle Z(\pi)\rangle} \tag{6·6}$$

according to the Z of the track recoiling against the D^+; the weight is 0 on average for pions and 1 for kaons. In the kaon projection, we find an excess centered on 5.28 GeV. We have considered and ruled out a number of potential sources for this excess. The following are effects we have considered which could add a kaon or proton background in the region in question:

- $\Lambda_b \to D^-p$ decays have too low a yield.
- $\Lambda_b \to \Lambda_c(p\pi^+\pi^-)K^-$, which is not covered by the $\Lambda_c \to pK^-\pi^+$ veto, does not contribute appreciably in the D^+ mass window.
- $\Lambda_b \to (pK^-\pi^+)K^-$ (non-resonant) is too small a contribution.
- Neither the $D_s^+K^-$ nor the Λ_cK^- reflection has the right mass.
- Finally, we have looked for $\overline{B}^0 \to D^+\pi^-$ candidates in Monte Carlo where the K_D^- and the π_B^- are swapped and still pass the D^+ mass cut; this effect occurs with negligible frequency ($<$ 10/50000 MC events).

Decay modes	Mass pdf	dE/dx pdf	fit parameters
		$\overline{B}^0 \to D^+\pi^-$ fit	
$\overline{B}^0 \to D^+\pi^-$	MC	prompt $D^* \to \pi$, $s:p$ reweight	norm floating
$\overline{B}^0 \to D^+\pi^-(n\gamma)$	MC	prompt $D^* \to \pi$, $s:p$ reweight	norm floating
$\overline{B}^0 \to D^+K^-$	MC	prompt $D^* \to K$, $s:p$ reweight	norm floating
$\overline{B}^0 \to D^+\rho^-$	MC	prompt $D^* \to \pi$, $s:p$ reweight	norm floating
$\overline{B}^0 \to D^{*+}\pi^-$	MC	prompt $D^* \to \pi$, $s:p$ reweight	norm floating
$D_2^*\pi^-$	MC	prompt $D^* \to \pi$, $s:p$ reweight	norm fixed to $\overline{B}^0/B^- \to D^+X$
$D^{(*)}K^{(*)}$	MC	prompt $D^* \to K$, $s:p$ reweight	norm fixed to $\overline{B}^0/B^- \to D^+X$
$D^{(*)}eX$	MC	parametric e simulation	norm fixed to $\overline{B}^0/B^- \to D^+X$
$\overline{B}^0/B^- \to D^+X$	MC	prompt $D^* \to \pi$, $s:p$ reweight	norm floating
$\overline{B}_s^0 \to D_s^+X$	MC	species fractions from MC	norm floating
D^+(sb) (fake-D bg)	D SB	D SB, signal-subtracted	norm floating, shape fixed
D^+X^+ (real-D bg)	WS (SBS)	WS (D signal region)	norm floating, shape fixed
		$\overline{B}^0 \to D^{*+}\pi^-$ fit	
$D^{*+}\pi^-$	MC	prompt $D^* \to \pi$, $s:p$ reweight	norm floating
$D^{*+}K^-$	MC	prompt $D^* \to K$, $s:p$ reweight	norm floating
$D^{*+}\rho^-$	MC	prompt $D^* \to \pi$, $s:p$ reweight	norm floating
$D^{*+}\pi^-(n\gamma)$	MC	prompt $D^* \to \pi$, $s:p$ reweight	norm floating
remainder ($D^{*+}X$)	MC	parametric simulation	norm floating
combinatorial bg	D^+ SB	D^+ SB	norm floating, shape fixed

Table 4: Fit components for $\overline{B}^0 \to D^+\pi^-$ and $\overline{B}^0 \to D^{*+}\pi^-$ fits. See the text for a description of the "mass pdf" and "dE/dx pdf" categories.

Decay modes	par no	Fit result			
		`xbhd0d`	`xbhd0h`	`xbhd0i`	comb
		$\overline{B}^0 \to D^+\pi^-$ fit			
$\overline{B}^0 \to D^+\pi^-$	2	4130.0 ± 81.2	5085.5 ± 89.6	4128.2 ± 80.8	13336.0 ± 145.4
$\overline{B}^0 \to D^+\pi^-(n\gamma)$	3	256.5 ± 67.0	231.5 ± 72.7	287.7 ± 68.3	734.5 ± 119.8
$\overline{B}^0 \to D^+K^-$	4	334.5 ± 31.0	526.4 ± 36.5	361.6 ± 31.8	1230.0 ± 57.6
$\overline{B}^0 \to D^+\rho^-$	5	2314.4 ± 290.2	4083.6 ± 321.6	2680.7 ± 286.9	8799.9 ± 519.2
$\overline{B}^0 \to D^{*+}\pi^-$	6	1406.3 ± 137.9	1302.4 ± 153.8	1331.0 ± 138.0	4118.4 ± 248.5
$D_2^*\pi^-$	7	fixed to $\overline{B}^0/B^- \to D^+X$			
$D^{(*)}K^{(*)}$	8	fixed to $\overline{B}^0/B^- \to D^+X$			
$D^{(*)}eX$	9	fixed to $\overline{B}^0/B^- \to D^+X$			
$\overline{B}^0/B^- \to D^+X$	10	2471.1 ± 165.6	2434.4 ± 183.1	2300.9 ± 165.3	7262.7 ± 296.6
$\overline{B}_s^0 \to D_s^+X$	11	715.9 ± 179.7	808.4 ± 194.5	644.8 ± 176.8	2156.9 ± 318.6
D^+(sb) (fake-D bg)	12	2376.1 ± 168.5	2855.9 ± 176.1	2105.2 ± 236.6	7361.2 ± 321.4
D^+X^+ (real-D bg)	13	333.3 ± 70.4	497.1 ± 79.4	494.9 ± 150.8	1498.5 ± 180.1
		$\overline{B}^0 \to D^{*+}\pi^-$ fit			
$D^{*+}\pi^-$	2	0.342 ± 0.009	0.367 ± 0.008	0.367 ± 0.009	0.359 ± 0.005
$D^{*+}K^-$	3	0.035 ± 0.005	0.028 ± 0.004	0.032 ± 0.004	0.032 ± 0.003
$D^{*+}\rho^-$	4	0.299 ± 0.021	0.287 ± 0.018	0.283 ± 0.020	0.287 ± 0.011
$D^{*+}\pi^-(n\gamma)$	5	0.030 ± 0.009	0.024 ± 0.008	0.025 ± 0.009	0.026 ± 0.005
remainder ($D^{*+}X$)	6	0.250 ± 0.020	0.255 ± 0.017	0.260 ± 0.019	0.257 ± 0.011
combinatorial bg		fixed to $1 - \sum_i f_i$			

Table 5: Fit parameters determined for $\overline{B}^0 \to D^+\pi^-$ and $\overline{B}^0 \to D^{*+}\pi^-$ by the combined mass and Z fit

Parameter		Correlation coefficients								
	global	2	3	4	5	6	10	11	12	13
2	0.52875	1.000	0.008	−0.014	0.157	0.015	0.025	−0.491	0.045	−0.024
3	0.59392	0.008	1.000	−0.341	−0.012	0.013	0.095	−0.254	−0.180	0.101
4	0.41565	−0.014	−0.341	1.000	0.051	−0.003	0.005	−0.016	−0.071	0.039
5	0.95049	0.157	−0.012	0.051	1.000	−0.823	−0.768	−0.253	−0.054	0.022
6	0.88356	0.015	0.013	−0.003	−0.823	1.000	0.659	−0.046	0.039	−0.009
10	0.87800	0.025	0.095	0.005	−0.768	0.659	1.000	−0.037	−0.152	0.046
11	0.83216	−0.491	−0.254	−0.016	−0.253	−0.046	−0.037	1.000	−0.244	0.129
12	0.87826	0.045	−0.180	−0.071	−0.054	0.039	−0.152	−0.244	1.000	−0.767
13	0.80764	−0.024	0.101	0.039	0.022	−0.009	0.046	0.129	−0.767	1.000

Table 6: Correlation coefficients for $\overline{B}^0 \to D^+\pi^-$ (combined 1.2 fb^{-1} fit)

Sample	$D^+K^-/D^+\pi^-$ (%)		$D^+\rho^-/D^+\pi^-$		$D^{*+}\pi^-/D^+\pi^-$	
PDG	6.80 ± 1.66		2.21 ± 0.68		0.81 ± 0.22	
`xbhd0d`	$8.03 \pm 0.81 \pm 0.22$	(0.66σ)	2.10 ± 0.26	(-0.15σ)	1.21 ± 0.13	(1.56σ)
`xbhd0h`	$10.43 \pm 0.81 \pm 0.28$	(1.95σ)	3.05 ± 0.25	(1.17σ)	0.93 ± 0.11	(0.46σ)
`xbhd0i`	$8.62 \pm 0.82 \pm 0.23$	(0.98σ)	2.41 ± 0.26	(0.29σ)	1.14 ± 0.12	(1.29σ)
comb	$9.21 \pm 0.47 \pm 0.25$	(1.38σ)	2.49 ± 0.15	(0.40σ)	1.11 ± 0.07	(1.26σ)
	$D^{*+}K^-/D^{*+}\pi^-$ (%)		$D^{*+}\rho^-/D^{*+}\pi^-$			
PDG	7.76 ± 0.45		2.46 ± 0.38			
`xbhd0d`	$9.59 \pm 1.49 \pm 0.26$	(1.16σ)	3.37 ± 0.31	(1.86σ)		
`xbhd0h`	$7.39 \pm 1.11 \pm 0.20$	(-0.31σ)	3.08 ± 0.25	(1.37σ)		
`xbhd0i`	$8.39 \pm 1.27 \pm 0.22$	(0.46σ)	3.02 ± 0.27	(1.21σ)		
comb	$8.39 \pm 0.73 \pm 0.22$	(0.71σ)	3.13 ± 0.16	(1.62σ)		

Table 7: Comparison with PDG for $\overline{B}^0 \to D^+\pi^-$ and $\overline{B}^0 \to D^{*+}\pi^-$ fits. The results are corrected for kinematic and XFT efficiency. For the $DK/D\pi$ ratio, the first error is statistical and the second is due to the XFT efficiency correction. The numbers in parentheses indicate the deviation from the PDG value.

Channels	Pull mean (%)	Pull width (%)
$B^0 \to D^-\pi^+$	-2.194 ± 1.006	99.631 ± 0.729
$B^0 \to D^-\pi^+(n\gamma)$	-0.726 ± 1.001	99.500 ± 0.716
$B^0 \to D^-K^+$	-1.450 ± 1.004	99.887 ± 0.713
$B^0 \to D^-\rho^+$	-1.406 ± 1.027	102.151 ± 0.730
$B^0 \to D^{*-}\pi^+$	1.101 ± 1.026	101.983 ± 0.734
$B^0/B^+ \to D^-X$	0.825 ± 1.024	101.908 ± 0.724
$B_s \to D_sX$	0.753 ± 1.012	100.605 ± 0.721
D^-(sb)	-0.847 ± 1.022	101.772 ± 0.725
D^-X^-	-1.340 ± 1.025	101.809 ± 0.734

Table 8: Pull distributions for $\overline{B}^0 \to D^+\pi^-$

We also note that both protons and kaons have a wider Z distribution than the bump we observe.

We have also considered effects which could deform the pion Z template with respect to the pions in data. We have checked for a secance dependence on mass, which we did not find. A comparison of the track parameters of tracks selected from the appropriate mass and Z region shows no difference with tracks from the appropriate mass region with no Z requirement.

A useful clue in this mystery is the absence of a discrepancy in the $D^{*+}\pi^-$ fit. Is the difference between D^+ and D^{*+} the absence of combinatorial background or the absence of statistics? To answer this question, add the bump observed in $D^+\pi^-$ to the pion Z template used in the $D^{*+}\pi^-$ fit. The χ^2 of the Z projection of the fit in the 5.26 GeV $< m(B) <$ 5.4 GeV region increases from 12.6 before the template modification to 24.0 after. The corresponding probabilities are 99% and 29%. Since $\Delta\chi^2$ is large but the χ^2 probability is still adequate, this study is inconclusive. In the next section, we choose treat the bump as a discrepancy between pions from $\overline{B}^0 \to D^+\pi^-$ and the pions template for the purpose of estimating the systematic uncertainty due to the bump.

6.5 Systematic Uncertainties

In this section we describe the various studies performed to determine the systematic uncertainties on $\mathcal{B}(\overline{B}^0 \to D^+K^-)/\mathcal{B}(\overline{B}^0 \to D^+\pi^-)$. Table 9 summarizes the systematic uncertainties.

6.5.1 Combinatorial background mass shape

Our knowledge of the combinatorial background mass shape is imperfect. We assess the systematic uncertainty associated with the background shape by comparing different background models. The default model uses two parameterized background components whose shapes are determined by fits to the two background samples ("fake-D + track" from the right-sign D sidebands and "real-D + track" from the wrong-sign D peak), letting the normalizations of both components float. There are multiple possibilities for alternate models; we choose a model that is both physically motivated and does not introduce a destabilizing number of additional fit parameters. This alternate model fixes the normalization of the fake-D background to the value determined in the D mass fit, as described in Section 6.1.2; to compensate for the loss of a parameter, it lets the shape parameters of the wrong-sign function float instead. We let the fitter determine values for the parameters of this model. These parameters are then used to generate toy MC. This toy MC is fit with the default model. The average over the pseudo-experiments of the difference between the measured and input $DK/D\pi$ ratio is -0.17. We use this as the systematic uncertainty due to the background mass model.

6.5.2 Monte Carlo smearing and scaling

As explained in Section 4, it is necessary to scale and smear the Monte-Carlo mass templates to achieve agreement with the data. We assess the systematic uncertainty associated with the errors on the scale factor by generating data with the scale factor varied up and down within the error. We use the greater of the changes in fit value resulting from an upward or downward variation as the systematic uncertainty due to the scale factor. The same method is employed to determine the systematic uncertainty due to the smearing.

6.5.3 dE/dx templates

We use several approaches to study the systematics associated with the dE/dx templates. First, as described in Section 5.2, the reweighting of the templates can be performed in several variables, each of which is a plausible proxy variable for the local hit density. The default fit uses secance, which is the most "local" of the variables we have studied: it attempts to measure the chamber activity in the vicinity of the track. A variable which behaves almost as well in reducing the difference between prompt and non-prompt templates is the total number of tracks n_{tr} in the event; this is also the most "global" conceivable proxy for the chamber activity. We generate toy MC with the n_{tr}-reweighted dE/dx templates and fit with the secance-reweighted templates. The average over the pseudo-experiments of the difference between the measured and input $DK/D\pi$ ratio is -0.31. We use this as the systematic uncertainty due to the choice of reweighting variable.

6.5.4 D_sX and fake-D species composition

Two other sources of systematic uncertainty are a result of the species composition of the D_sX Z template and the fake-D Z template. We assess the systematic uncertainty due to the K content of the D_sX Z template by reducing the K content by 50%. This covers the expected range of possible deviations of the $B_s \to D_sK$ branching fraction from the value in the generator table. We assess the systematic uncertainty due to the composition of the fake-D Z template by generating toy MC with a fake-D Z template on which no signal subtraction has been performed.

6.5.5 Z residuals in the $D^+\pi^-$-dominated region

The final dE/dx systematic uncertainty assessment quantifies the effect of the bump in the Z residuals in the $D^+\pi^-$-dominated region. We add the difference between data and fit in the region 5.26 GeV $< m(B) <$ 5.4 GeV to the $D^+\pi^-$ and $D^+\pi^-(n\gamma)$ templates. We generate toy MC with these templates and fit with the default templates. The average over the pseudo-experiments of the difference between the measured and input $DK/D\pi$ ratio is -0.45. We use this as the systematic uncertainty due to the bump in the Z residuals. Since

Effect	$D^+K^-/D^+\pi^-$ (fit − generated) (%)
Combinatorial bg model	−0.17
Scale factor (mean−1σ)	0.15
Smearing (mean+1σ)	0.16
Z reweighting in $n_{\mathrm{tr}} : p$	−0.31
Bump in π Z template	−0.45
K fraction in D_sX Z template	0.16
Signal subtraction in fake-D Z template	−0.30
Sum in quadrature	0.70

Table 9: Systematic uncertainties on $\mathcal{B}(\overline{B}^0 \to D^+K^-)/\mathcal{B}(\overline{B}^0 \to D^+\pi^-)$

the source of the discrepancy is unknown, the systematic in other samples will have to be assessed based on the size of the discrepancy (if any) in those samples.

6.6 Comparison with PDG

Table 7 compares our fit result in each of the subsamples to the PDG values. To explain the discrepancy between our value for $\mathcal{B}(\overline{B}^0 \to D^+K^-)/\mathcal{B}(\overline{B}^0 \to D^+\pi^-)$ and the previous Belle measurement [16], we would like to draw the reader's attention to the fit in Fig. 1(d) of [16], on which the Belle measurement is based. We believe this fit (based on approximately 30 D^+K^- events) can accommodate our result.

7 $\overline{B}^0 \to D^{*+}\pi^-$ Fit

In this section we apply the fit to the $\overline{B}^0 \to D^{*+}\pi^-$ sample. We describe the fit configuration, the fit results and the agreement with PDG. (Because this sample is much cleaner than the signal samples, we believe there is nothing valuable to be learned from estimating systematic uncertainties.)

7.1 Configuration

The fit is a non-extended unbinned maximum-likelihood fit. The $D^*\pi$ mass is calculated with the D^0 mass constrained to the PDG value. Table 4 lists the fit components. The mass templates marked "Monte Carlo" are selected from single-B Monte Carlo according to the decay channels shown in the table. The Monte-Carlo candidate sets used in the single-B templates are disjoint; the templates are listed in order of precedence.

Parameter	global	Correlation coefficients 2	3	4	5	6
2	0.72894	1.000	−0.103	−0.134	0.204	−0.173
3	0.55815	−0.103	1.000	0.038	0.400	−0.035
4	0.92648	−0.134	0.038	1.000	0.199	−0.829
5	0.72548	−0.204	−0.400	−0.199	1.000	0.002
6	0.92304	−0.173	−0.035	−0.829	0.002	1.000

Table 10: Correlation coefficients for $\overline{B}^0 \to D^{*+}\pi^-$ (combined 1.2 fb^{-1} fit)

Because the combinatorial background under the D^{*+} is small, we cannot extract the background shape parameters from the data. We instead use the shape parameters of the fake-D background in the D^+ fit. These parameters are fixed in the $\overline{B}^0 \to D^{*+}\pi^-$ fit. Since the background is small, the fit results are robust to background mis-parameterization.

The Z templates marked "prompt D^*" in Table 4 are described in Section 5.2 and [12]. Two-dimensional reweighting in secance and momentum is applied. The Z template for the "remainder" background is obtained from the parametric dE/dx simulation described in Section 5.2.

7.2 Results

Results of the likelihood fit are given in Table 5. Mass projections are shown in Figures 30–33. Z projections are shown in Figures 38–41. The likelihood scan in each fit variable is shown in Figure 44.

The results returned by the fitter are corrected for the relative efficiencies of the different channels as described in Section 6.2. Table 7 shows the results.

7.3 Fitter Validation

We cross-check the fit by plotting the pull distributions of the fit parameters. Data is generated by throwing dice against the mass and dE/dx templates with the f_j determined in the fit as the "true" f_j. The data is then fit. Figure 45 shows that the fit provides unbiased results and that the error estimate is correct. Table 11 lists the pull means and widths for 10000 pseudoexperiments of 9664 events each. The combinatorial background fraction is not a fit parameter, and so its error is not returned by the fit; instead we calculate it by propagating the errors on the fit parameters as follows:

$$\sigma_{\rm bg}^2 = \sum_{i,j}^{M-1} \sigma_{ij}, \tag{7·1}$$

Channels	Pull mean (%)	Pull width (%)
$D^{*+}\pi^-$	0.121 ± 1.015	100.638 ± 0.742
$D^{*+}K^-$	-5.114 ± 1.003	100.187 ± 0.713
$D^{*+}\rho^-$	-0.704 ± 1.005	100.472 ± 0.712
$D^{*+}\pi^-(n\gamma)$	-0.880 ± 1.011	100.989 ± 0.718
remainder	0.011 ± 1.003	100.258 ± 0.710
combinatorial background	-4.995 ± 1.003	100.130 ± 0.715

Table 11: Pull distributions for $\overline{B}^0 \to D^{*+}\pi^-$

where M is the number of fit components including the combinatorial background.

7.4 Comparison with PDG

Table 7 compares our fit result in each of the subsamples to the PDG values. The agreement in $\mathcal{B}(\overline{B}^0 \to D^{*+}K^-)/\mathcal{B}(\overline{B}^0 \to D^{*+}\pi^-)$ is good; this value is better known than the corresponding D^+ ratio thanks to a high-statistics BaBar measurement [17].

8 Conclusions

We conclude the following from the fits to the control samples. First, the fitter is unbiased and the error estimates are correct. Second, the fit components model the samples well. Third, the fit results are in good agreement with BaBar and Belle. Finally, we have developed the toy Monte Carlo mechanism required for determining systematic errors. We believe that this control sample analysis demonstrates that we are ready to proceed to the signal samples.

9 Figures

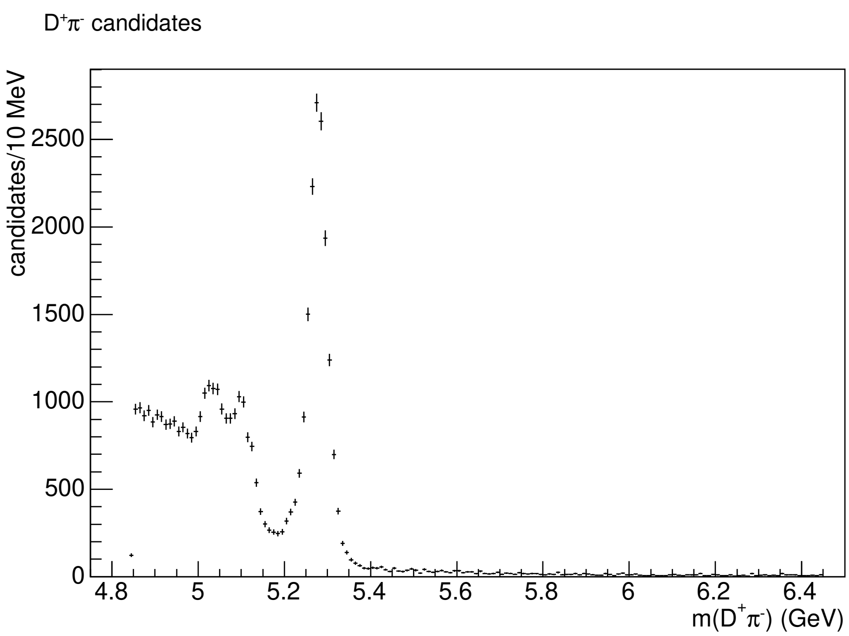

Figure 1: Mass distribution for $\overline{B}^0 \to D^+\pi^-$, $D^+ \to K^-\pi^+\pi^+$ candidates in the combined 1.2 fb^{-1} dataset

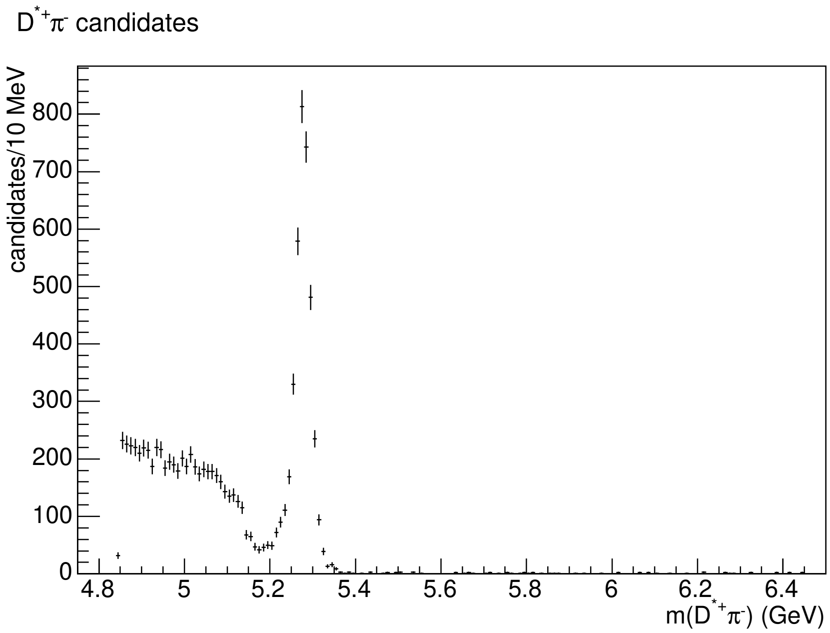

Figure 2: Mass distribution for $\overline{B}^0 \to D^{*+}\pi^-$, $D^{*+} \to D^0\pi^+$, $D^0 \to K^-\pi^+$ candidates in the combined 1.2 fb^{-1} dataset

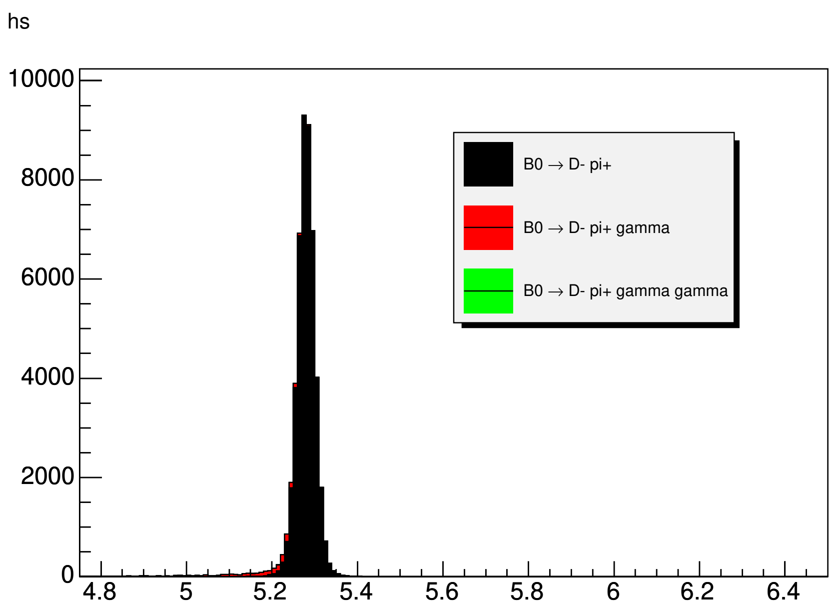

Figure 3: Composition of $\overline{B}^0 \to D^+\pi^-(n\gamma)$ Monte-Carlo sample reconstructed as $\overline{B}^0 \to D^+(K^-\pi^+\pi^+)\pi^-$

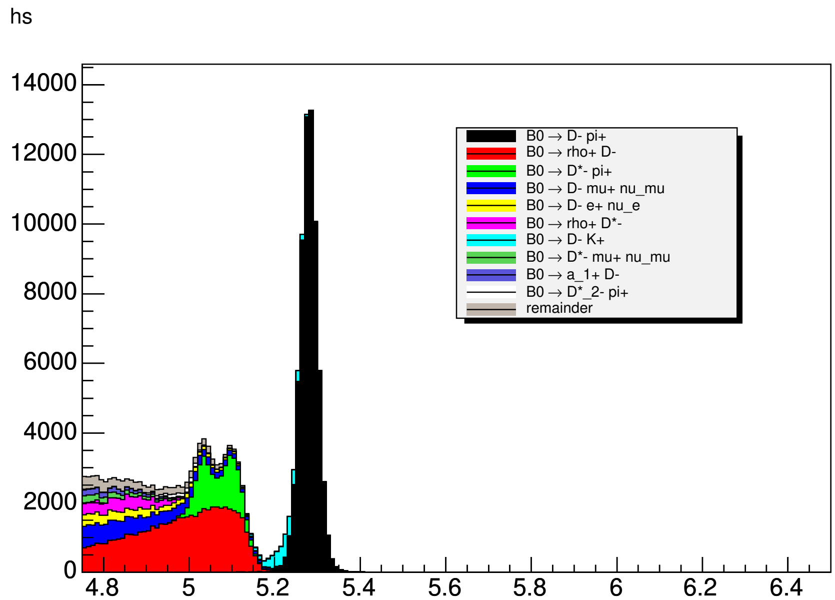

Figure 4: Composition of $\overline{B}^0 \to D^+X$ Monte-Carlo sample reconstructed as $\overline{B}^0 \to D^+(K^-\pi^+\pi^+)\pi^-$

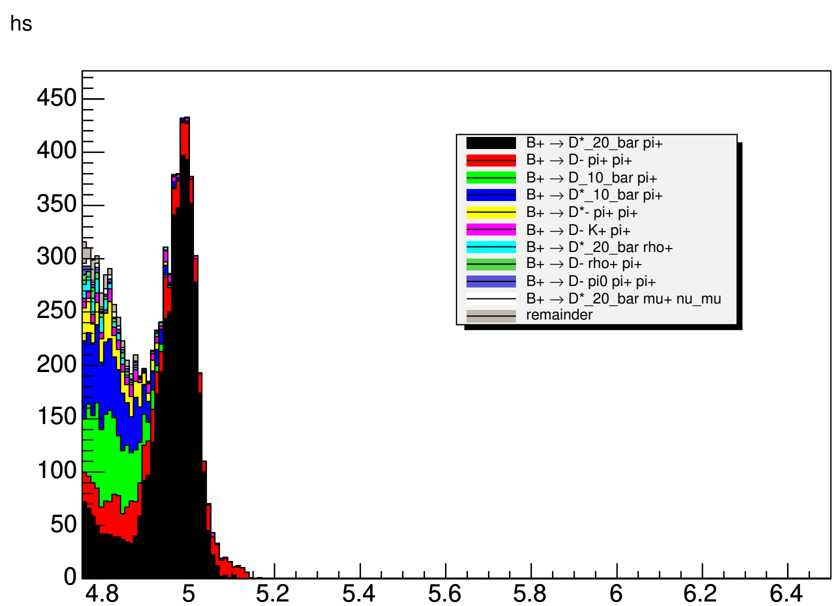

Figure 5: Composition of $B^- \to D^+X$ Monte-Carlo sample reconstructed as $\overline{B}^0 \to D^+(K^-\pi^+\pi^+)\pi^-$

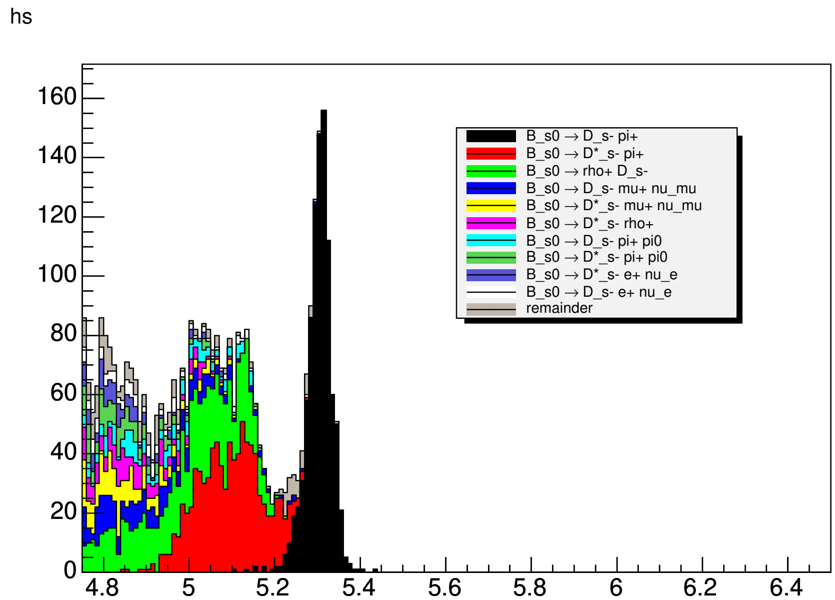

Figure 6: Composition of $B_s \to D_s(\phi\pi)X$ Monte-Carlo sample reconstructed as $\overline{B}^0 \to D^+(K^-\pi^+\pi^+)\pi^-$

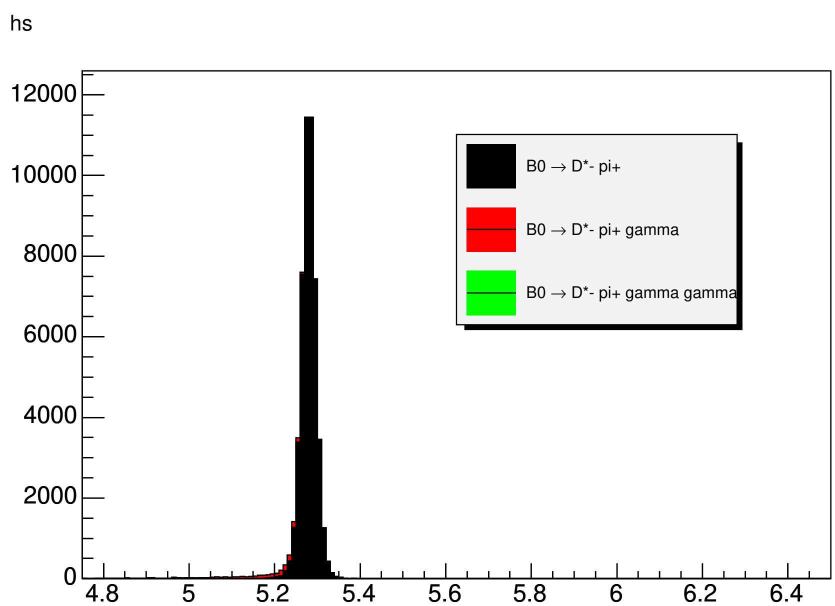

Figure 7: Composition of $\overline{B}^0 \to D^{*+}\pi^-(n\gamma)$ Monte-Carlo sample reconstructed as $\overline{B}^0 \to D^{*+}\,(D^0(K^-\pi^+)\pi^-)\,\pi^-$

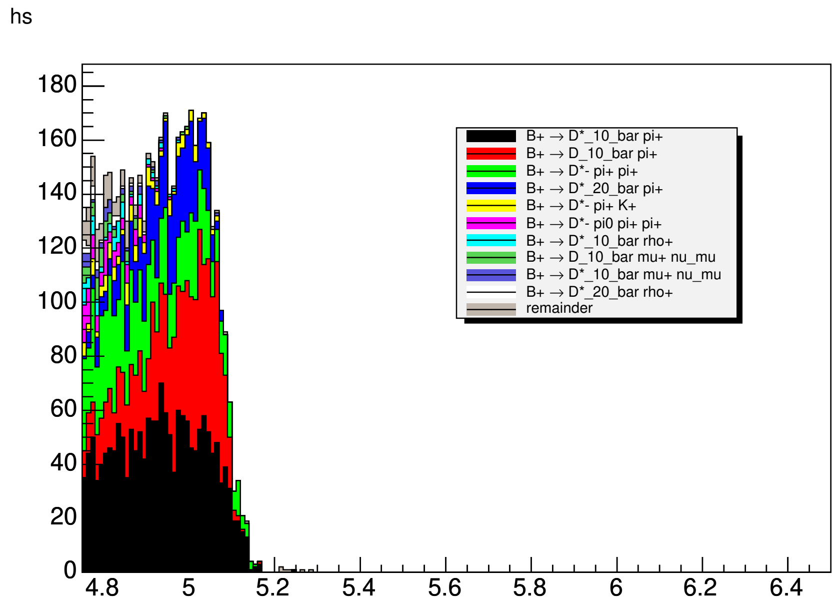

Figure 8: Composition of $B^- \to D^0\pi^- X$ Monte-Carlo sample reconstructed as $\overline{B}^0 \to D^{*+}\,(D^0(K^-\pi^+)\pi^-)\,\pi^-$

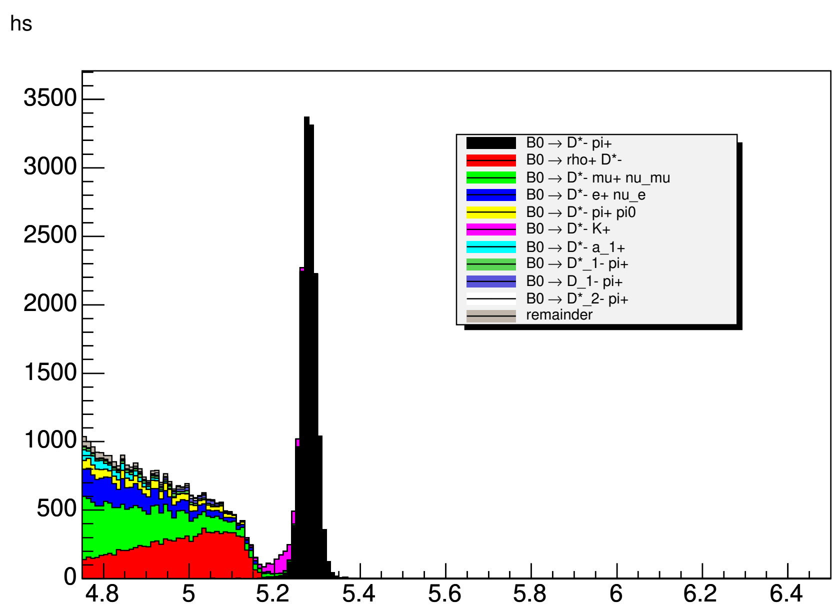

Figure 9: Composition of $\overline{B}^0 \to D^{*+}X$ Monte-Carlo sample reconstructed as $\overline{B}^0 \to D^{*+}\,(D^0(K^-\pi^+)\pi^-)\,\pi^-$

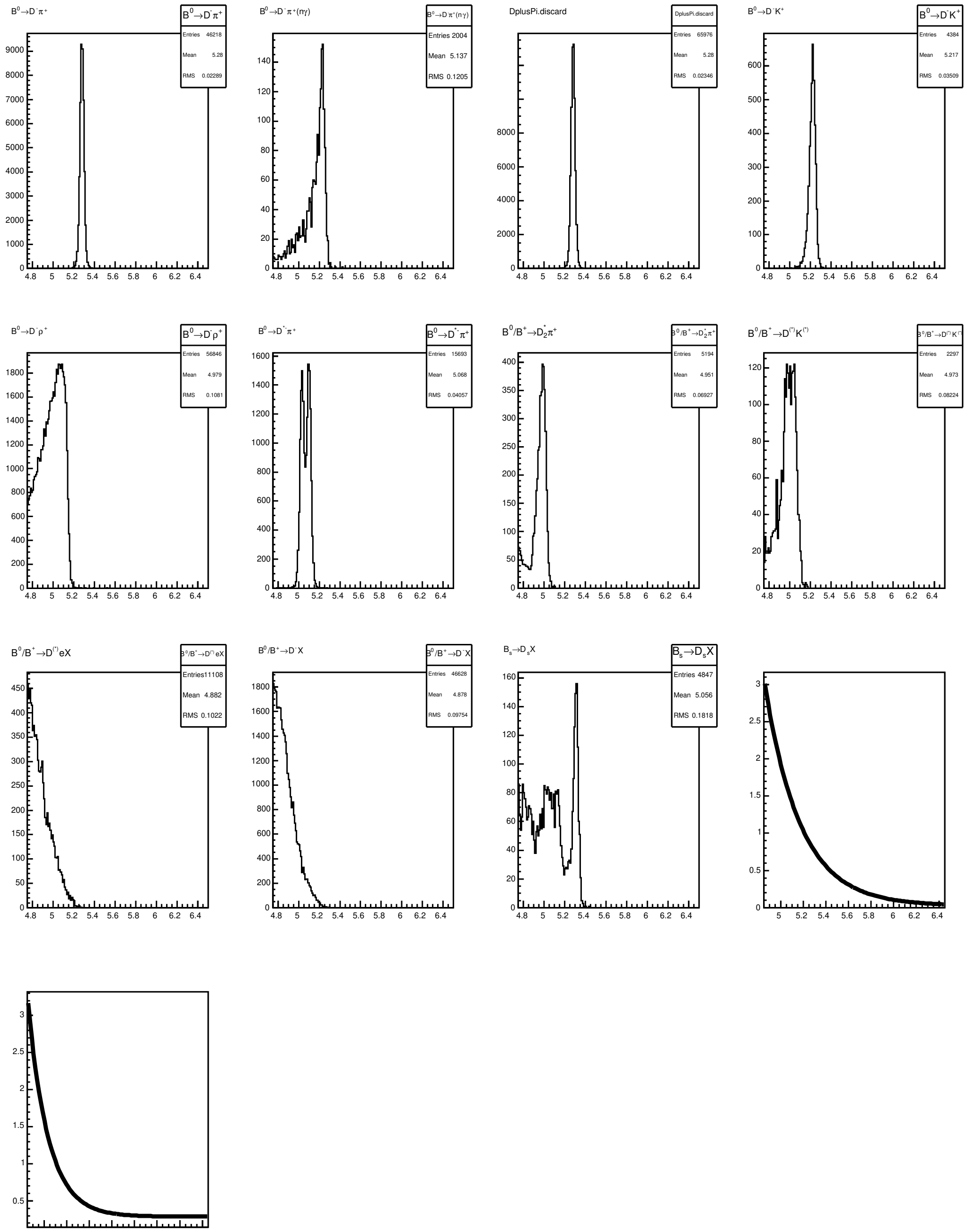

Figure 10: Mass templates used to model the $\overline{B}^0 \to D^+X$, $D^+ \to K^-\pi^+\pi^+$ fit components. The template marked "$\overline{B}^0 \to D^+\pi^-$.discard" is extracted from the non-PHOTOS Monte-Carlo sample to determine the $D^+K^-/D^+\pi^-$ relative yield, but is not used as a fit template.

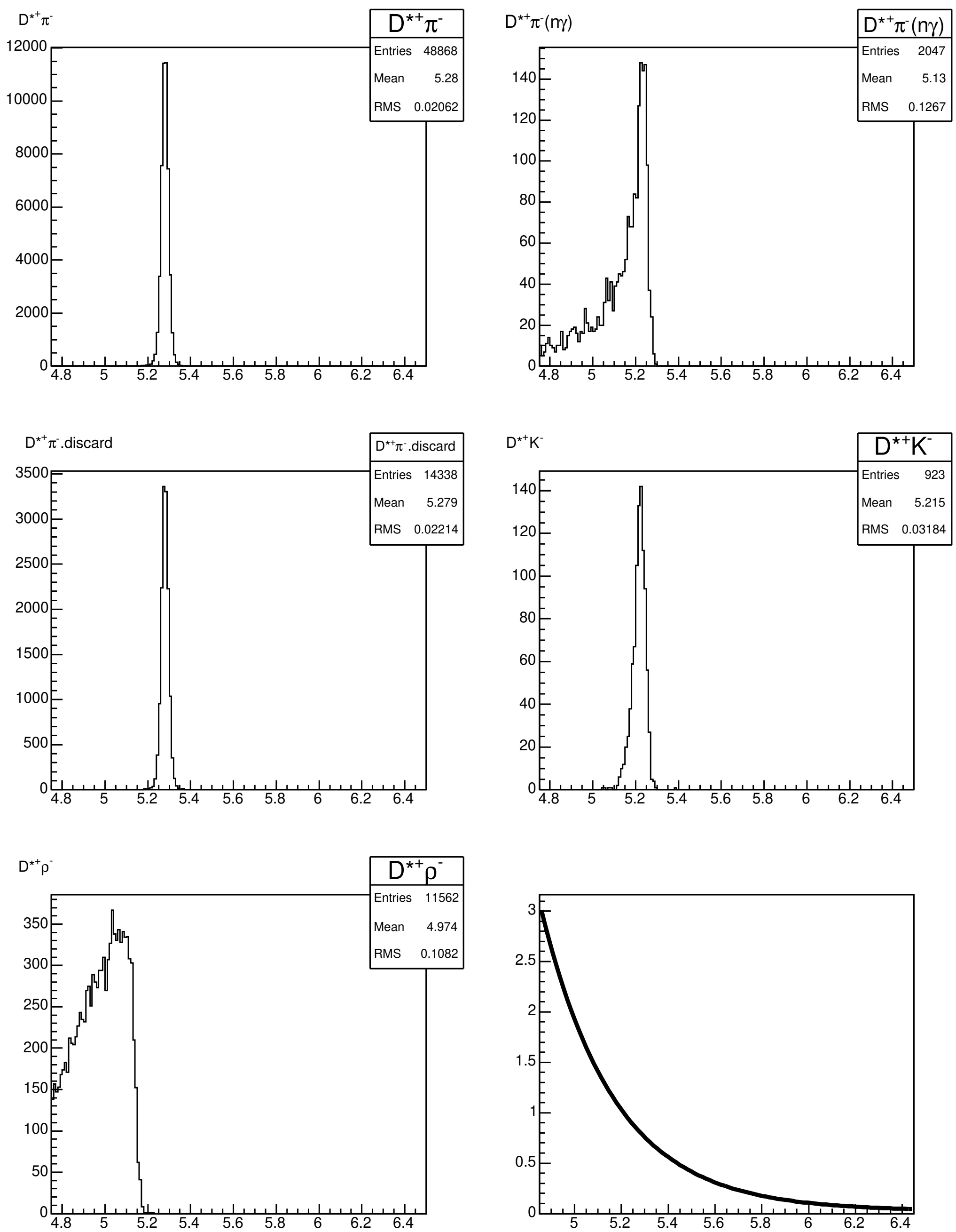

Figure 11: Mass templates used to model the $\overline{B}^0 \to D^{*+}X$, $D^{*+} \to D^0\pi^+$, $D^0 \to K\pi$ fit components. The template marked "$D^{*+}\pi^-$.discard" is extracted from the non-PHOTOS Monte-Carlo sample to determine the $D^{*+}K^-/D^{*+}\pi^-$ relative yield, but is not used as a fit template.

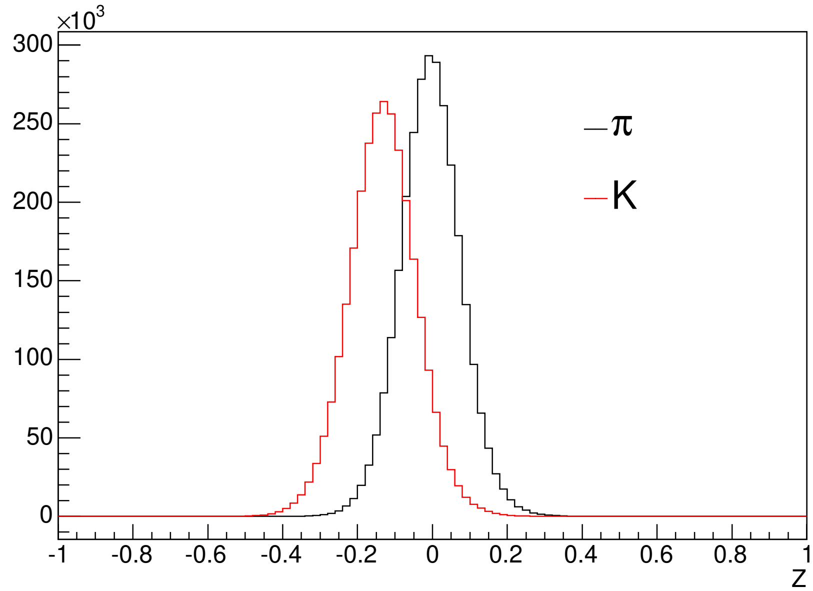

Figure 12: Z templates for K and π tracks reweighted for $\overline{B}^0 \to D^+ X$

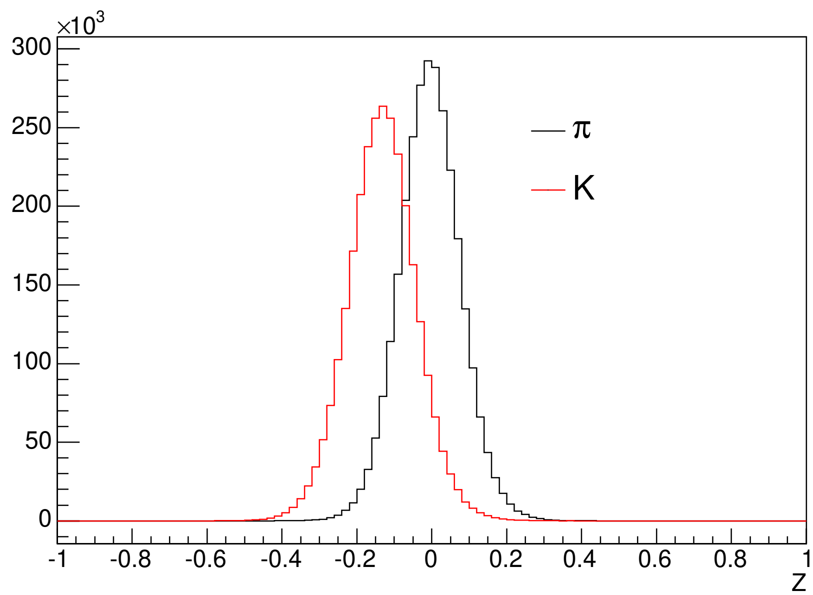

Figure 13: Z templates for K and π tracks in reweighted for $\overline{B}^0 \to D^{*+} X$

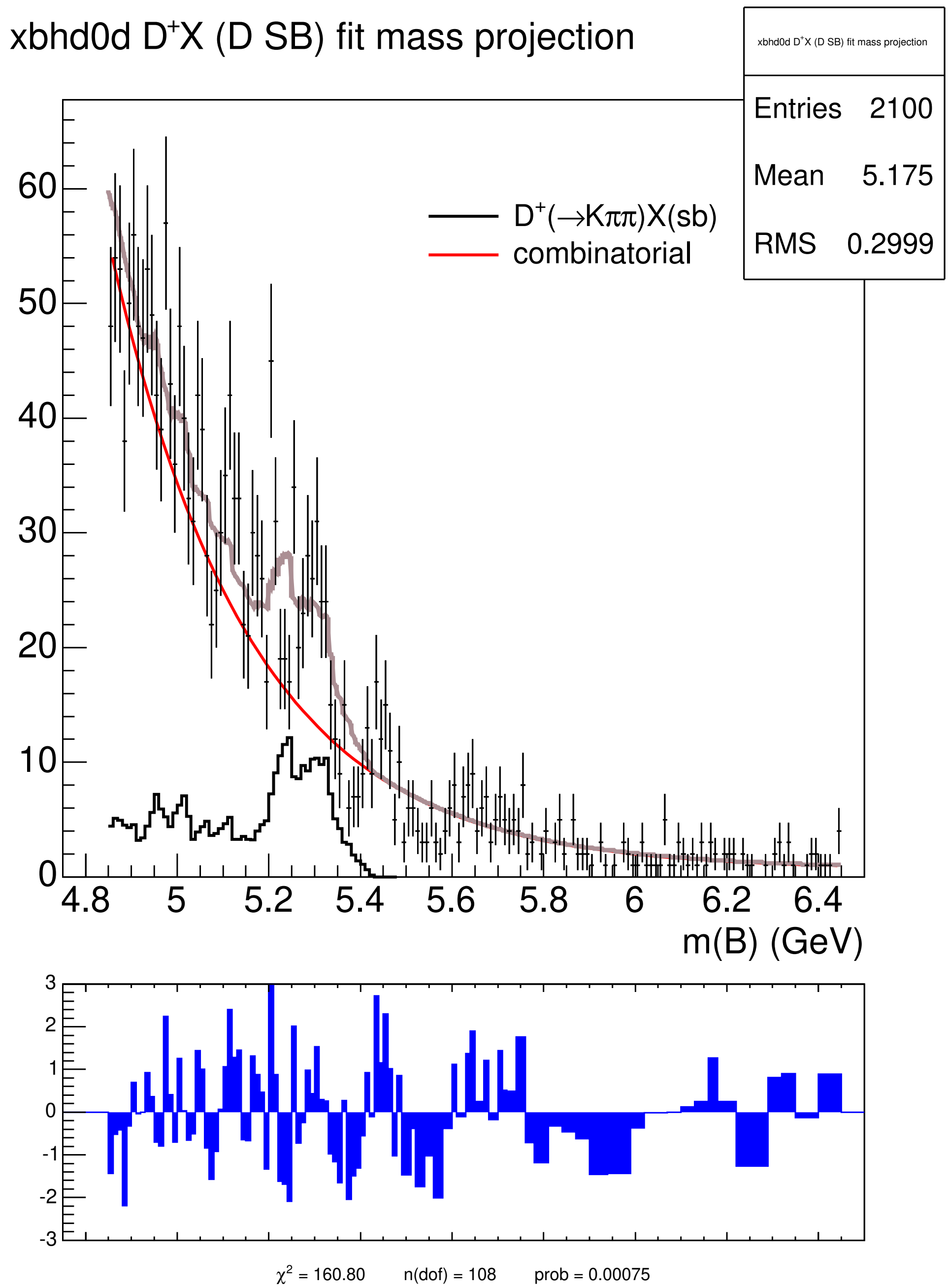

Figure 14: Fake-D^+ combinatorial template (`xbhd0d`). The histogram is obtained using the D^+ sidebands. The combinatorial background shape is an exponential plus a flat background of the form (5·4).

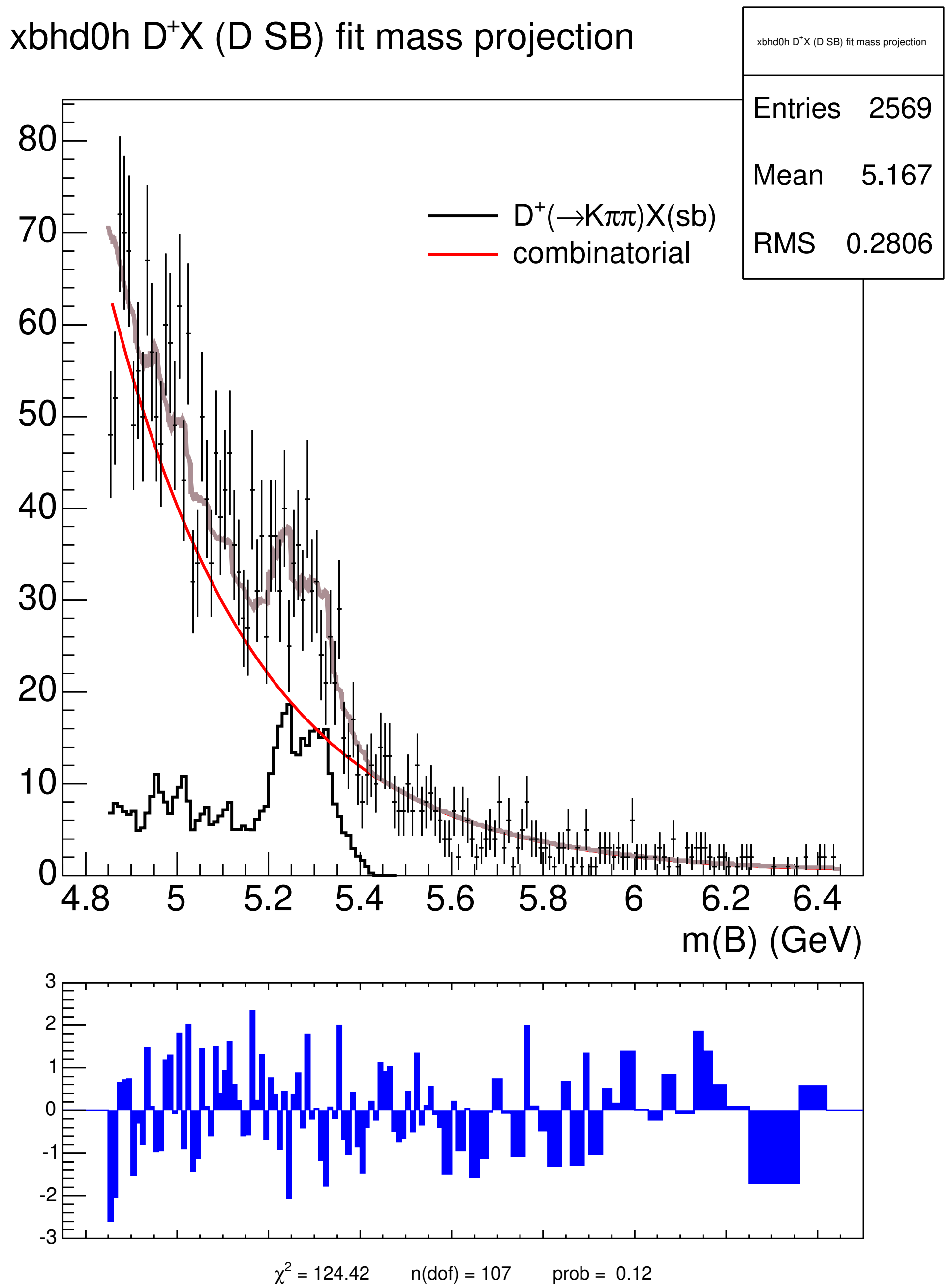

Figure 15: Fake-D^+ combinatorial template (`xbhd0h`). The histogram is obtained using the D^+ sidebands. The combinatorial background shape is an exponential plus a flat background of the form (5·4).

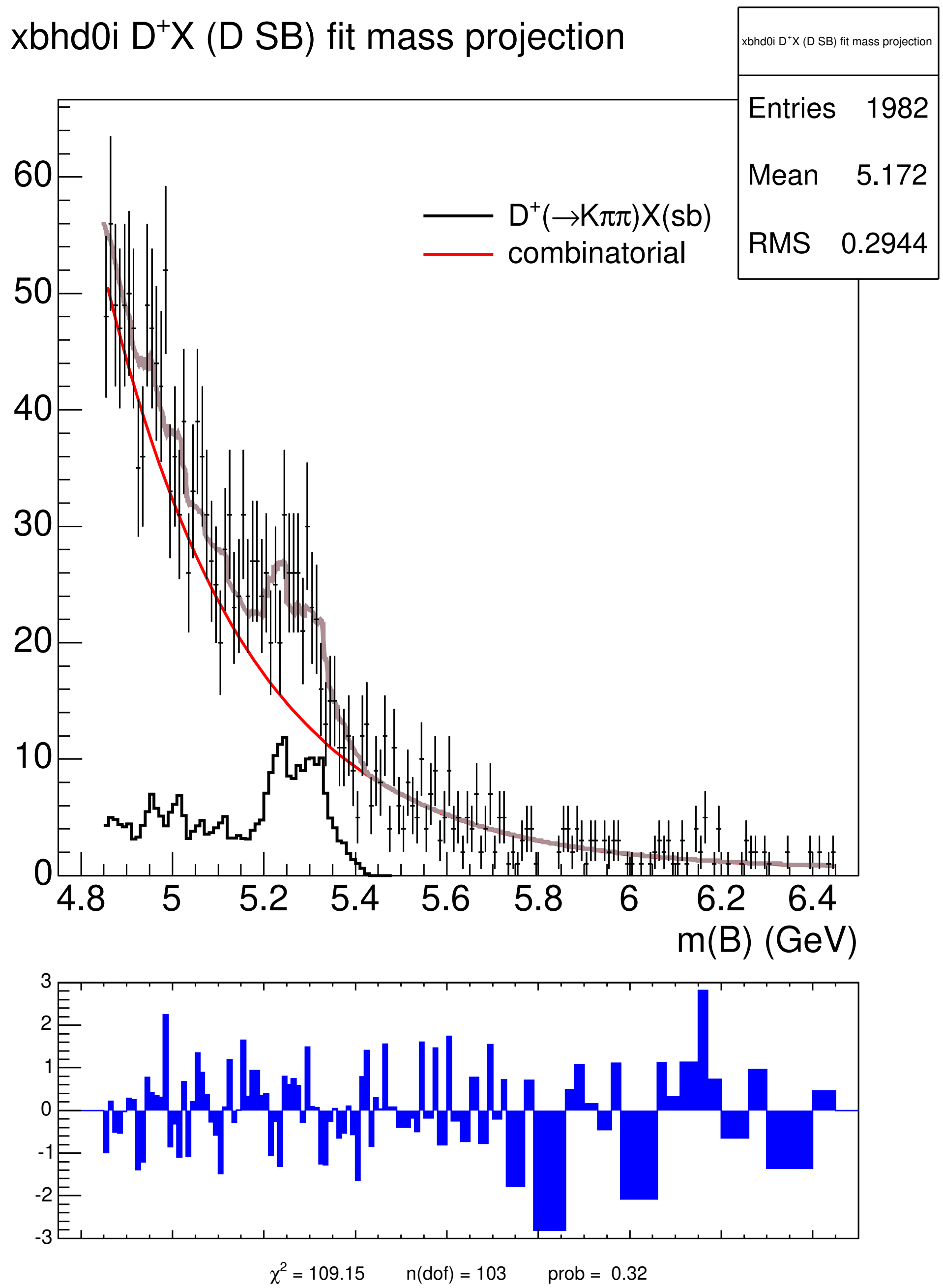

Figure 16: Fake-D^+ combinatorial template (`xbhd0i`). The histogram is obtained using the D^+ sidebands. The combinatorial background shape is an exponential plus a flat background of the form (5·4).

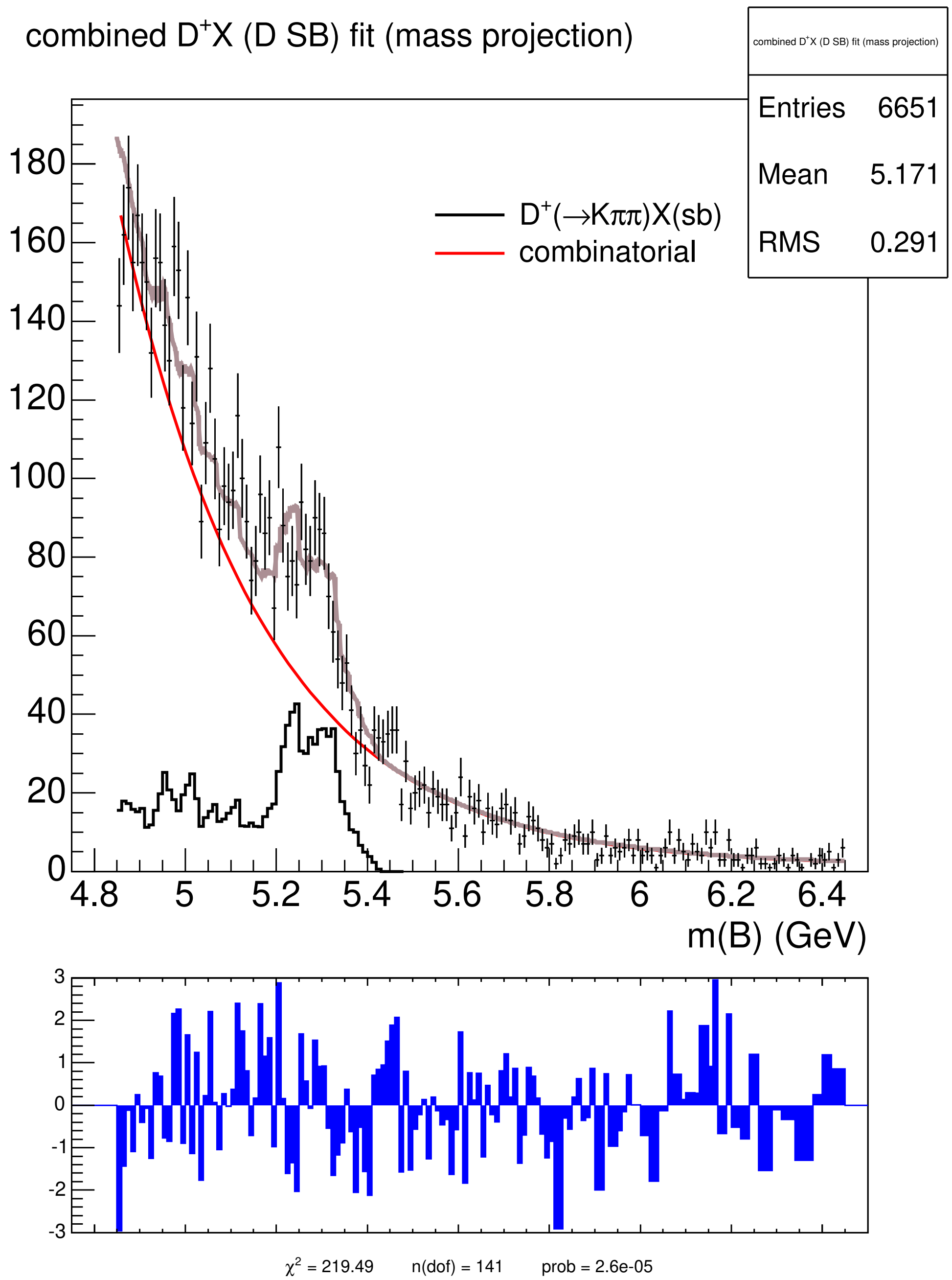

Figure 17: Fake-D^+ combinatorial template (combined). The histogram is obtained using the D^+ sidebands. The combinatorial background shape is an exponential plus a flat background of the form (5·4).

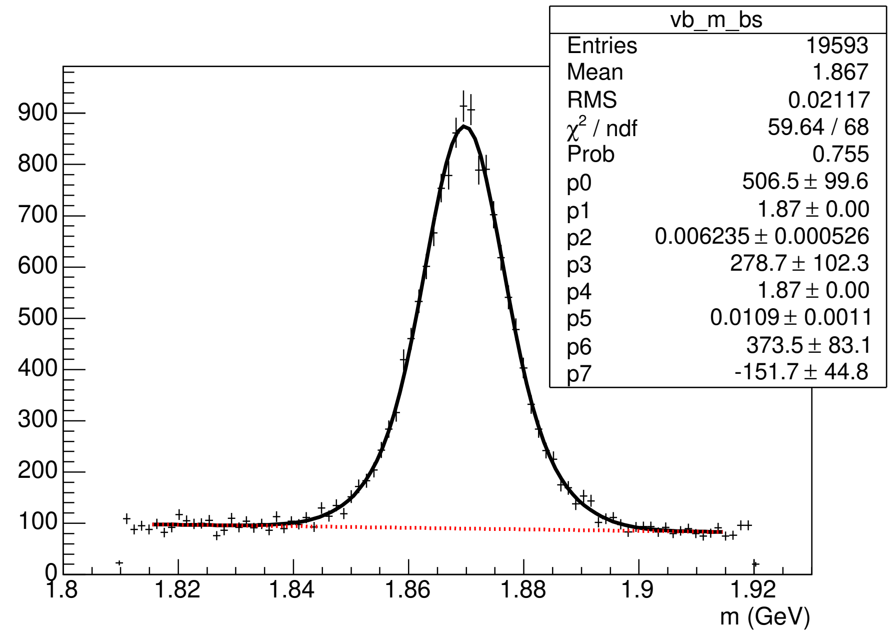

Figure 18: Fake-D^+ combinatorial normalization fit (`xbhd0d`)

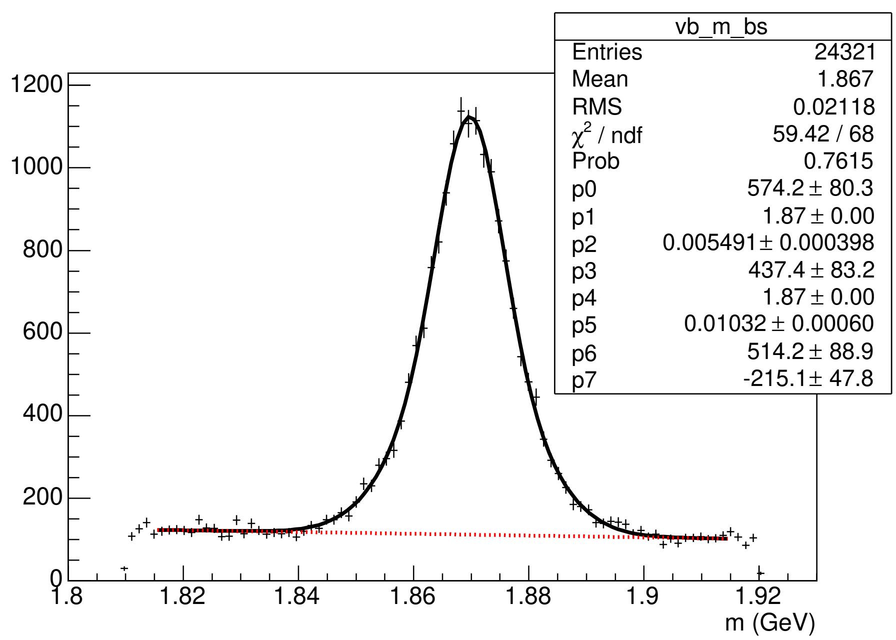

Figure 19: Fake-D^+ combinatorial normalization fit (`xbhd0h`)

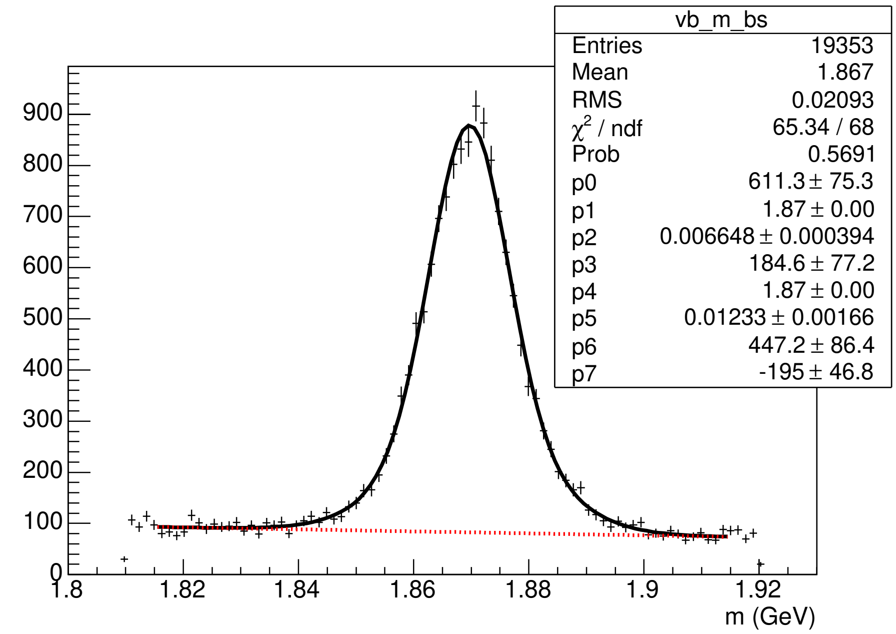

Figure 20: Fake-D^+ combinatorial normalization fit (`xbhd0i`)

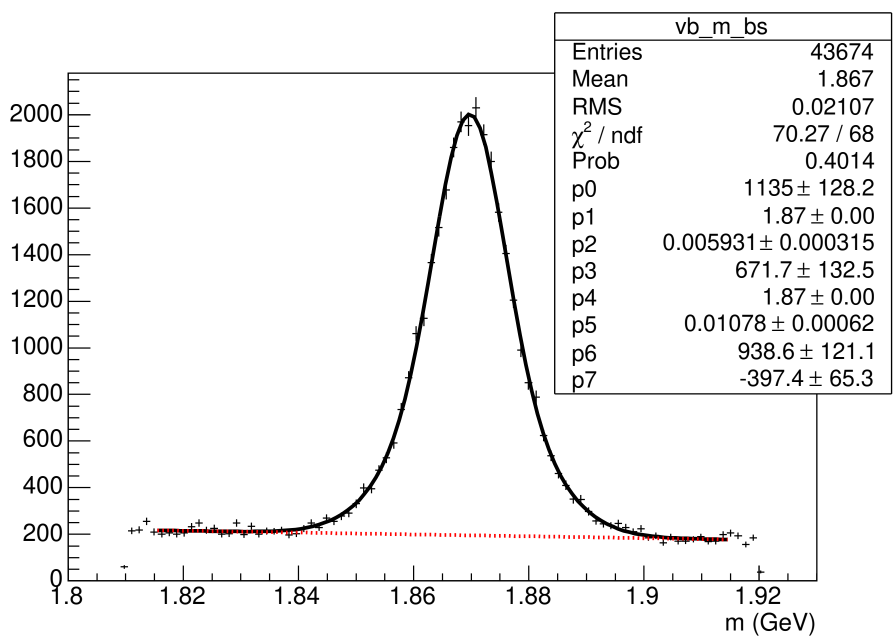

Figure 21: Fake-D^+ combinatorial normalization fit (combined)

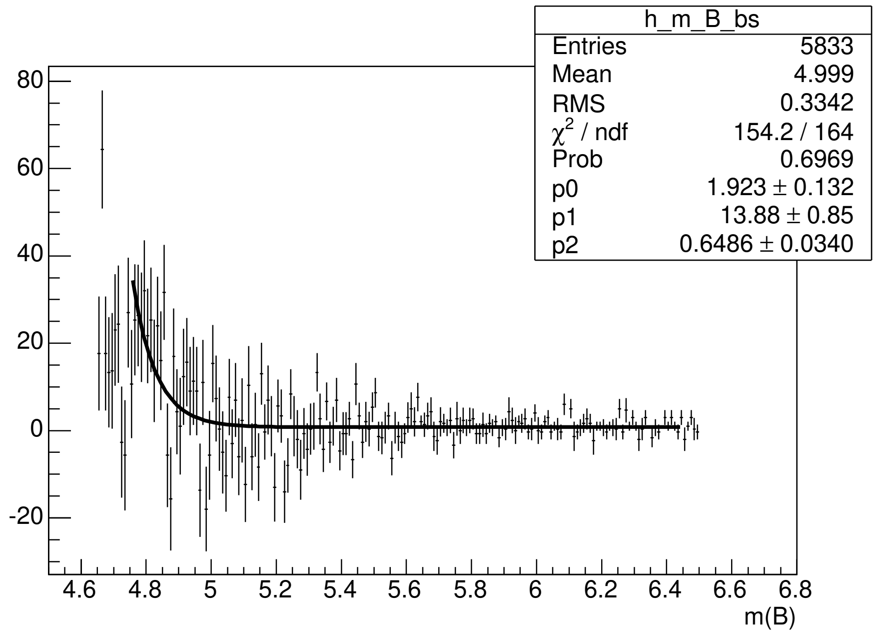

Figure 22: Real-D^+ combinatorial template fit (`xbhd0d`)

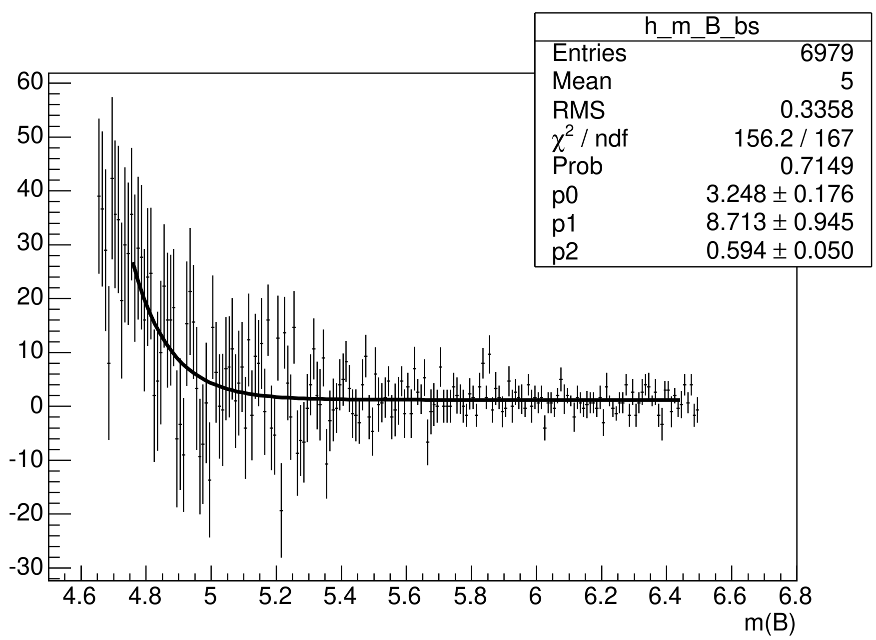

Figure 23: Real-D^+ combinatorial template fit (`xbhd0h`)

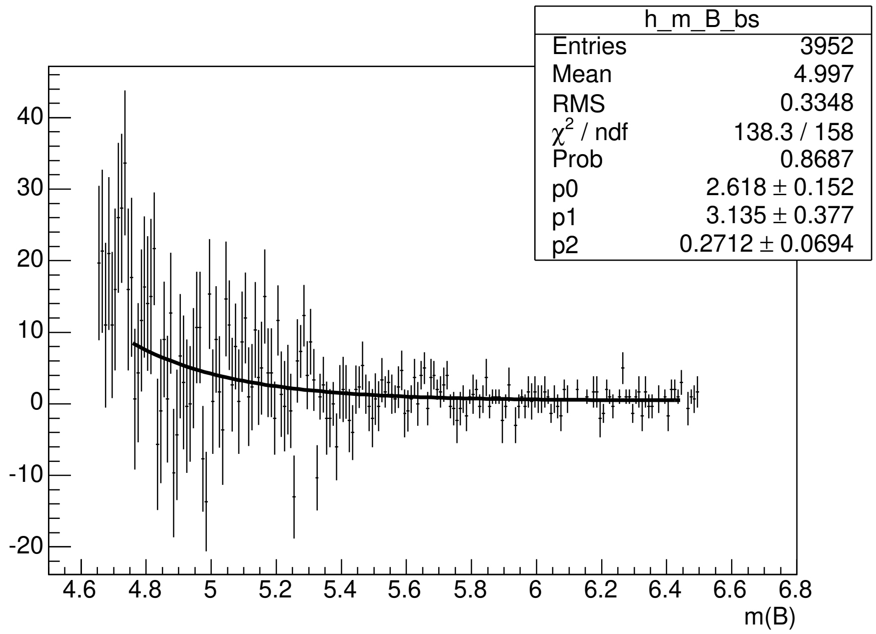

Figure 24: Real-D^+ combinatorial template fit (`xbhd0i`)

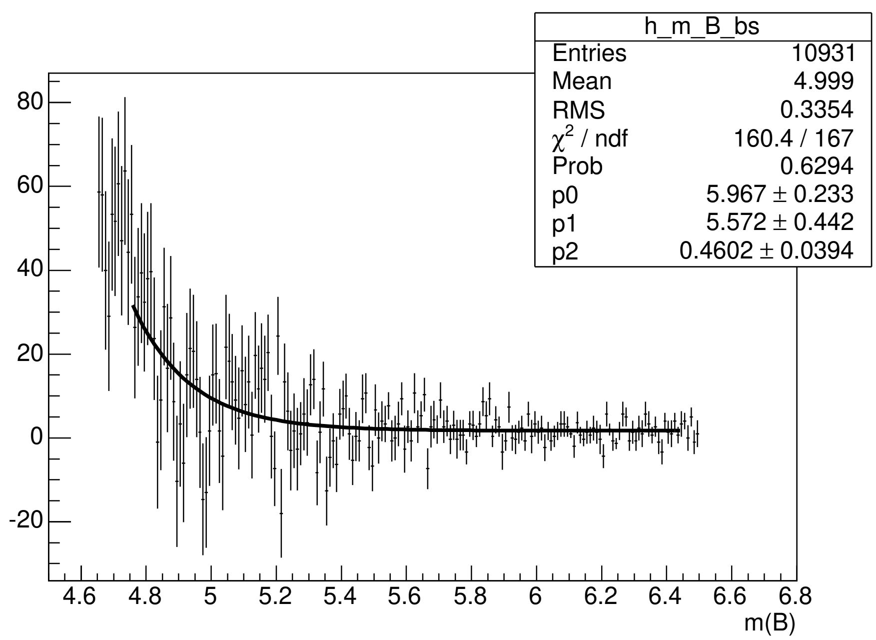

Figure 25: Real-D^+ combinatorial template fit (combined)

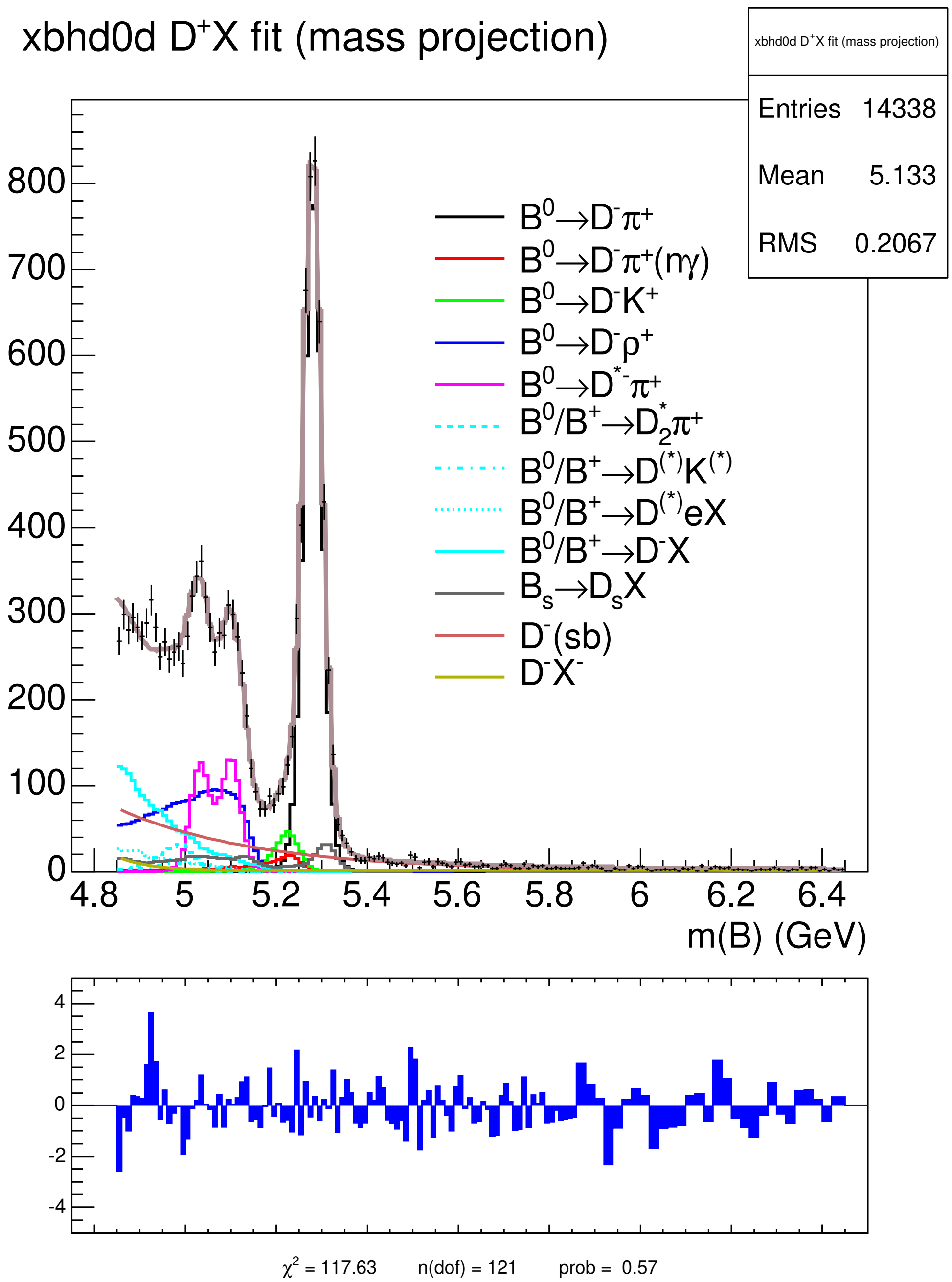

Figure 26: Mass projection of the likelihood fit results for $\overline{B}^0 \to D^+\pi^-$, $D^+ \to K^-\pi^+\pi^+$ candidates in `xbhd0d`. The residual plot at the bottom shows the number of σ discrepancy (data minus fit). In the calculation of the residuals, neighboring bins are combined until the predicted number of events is > 5.

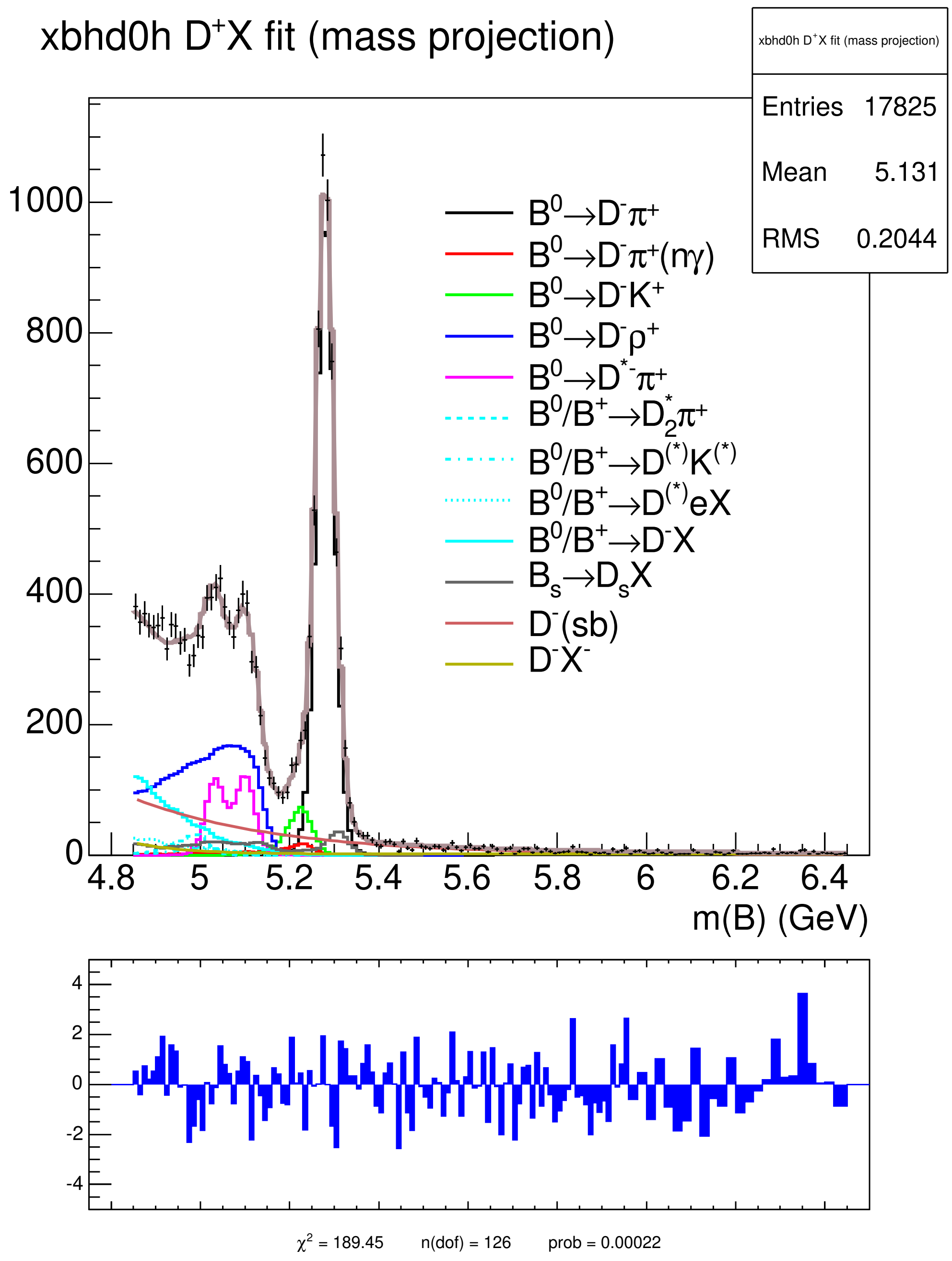

Figure 27: Mass projection of the likelihood fit results for $\overline{B}^0 \to D^+\pi^-$, $D^+ \to K^-\pi^+\pi^+$ candidates in `xbhd0h`. The residual plot at the bottom shows the number of σ discrepancy (data minus fit). In the calculation of the residuals, neighboring bins are combined until the predicted number of events is > 5.

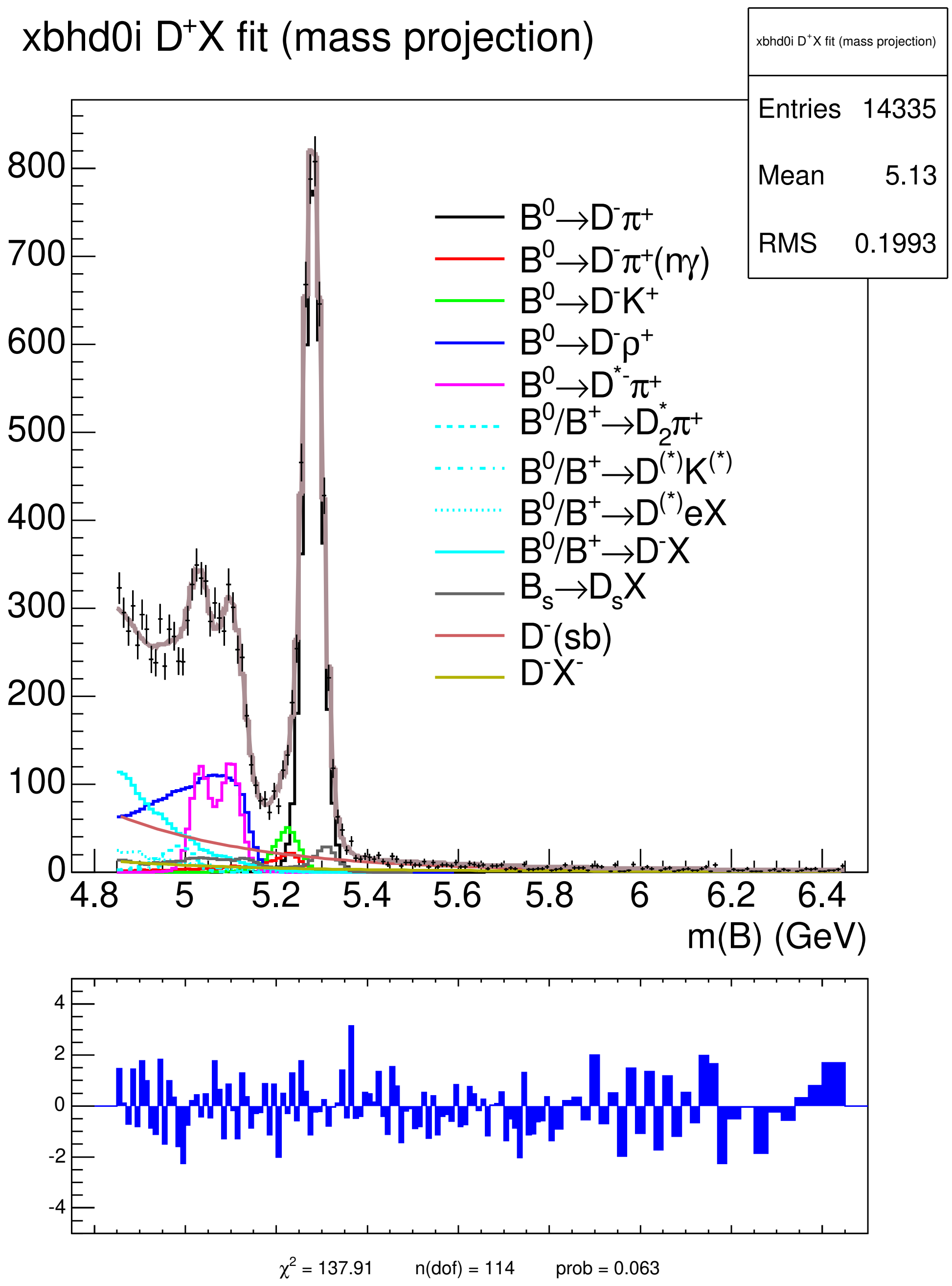

Figure 28: Mass projection of the likelihood fit results for $\overline{B}^0 \to D^+\pi^-$, $D^+ \to K^-\pi^+\pi^+$ candidates in `xbhd0i`. The residual plot at the bottom shows the number of σ discrepancy (data minus fit). In the calculation of the residuals, neighboring bins are combined until the predicted number of events is > 5.

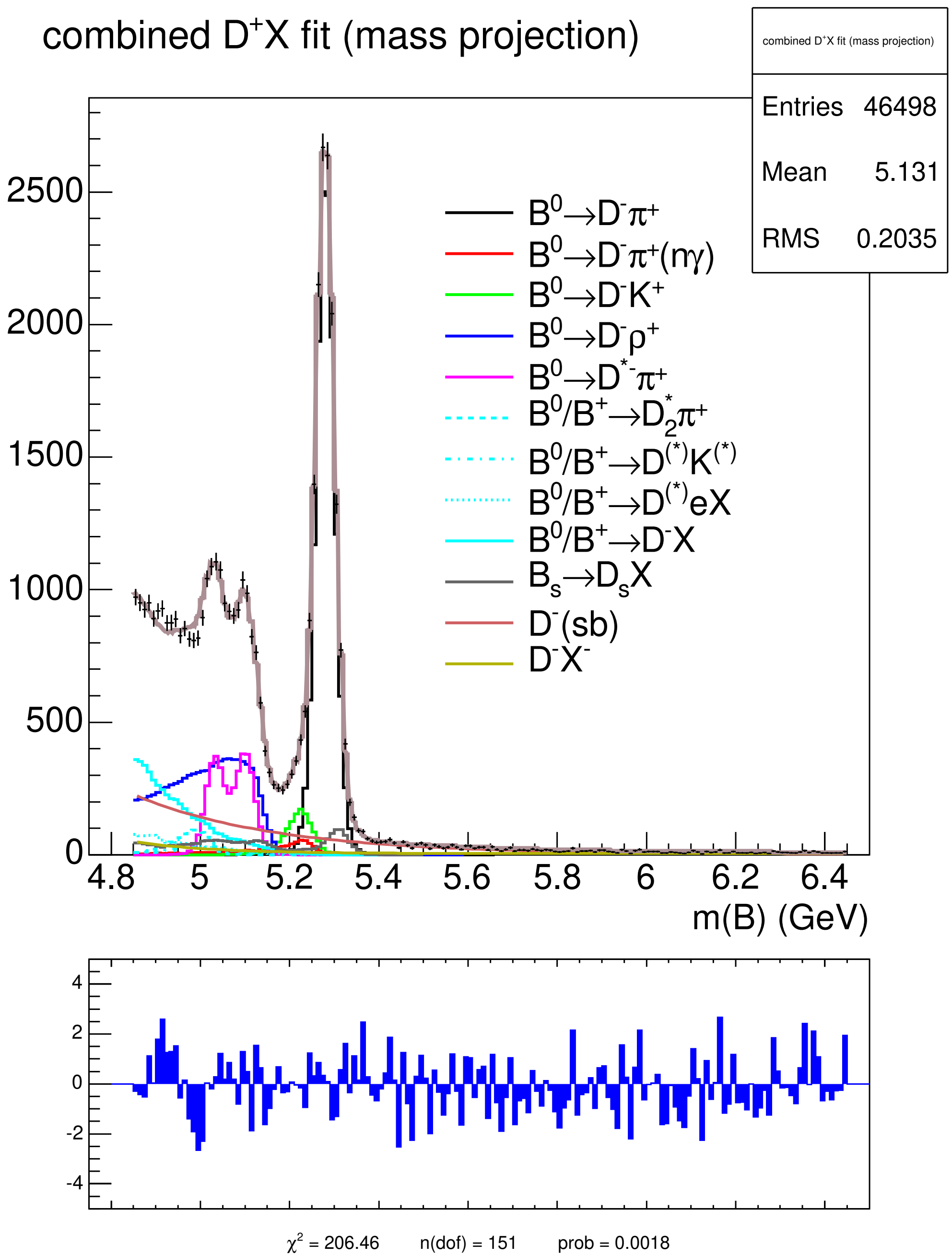

Figure 29: Mass projection of the likelihood fit results for $\overline{B}^0 \rightarrow D^+\pi^-$, $D^+ \rightarrow K^-\pi^+\pi^+$ candidates in the combined 1.2 fb^{-1}. The residual plot at the bottom shows the number of σ discrepancy (data minus fit). In the calculation of the residuals, neighboring bins are combined until the predicted number of events is > 5.

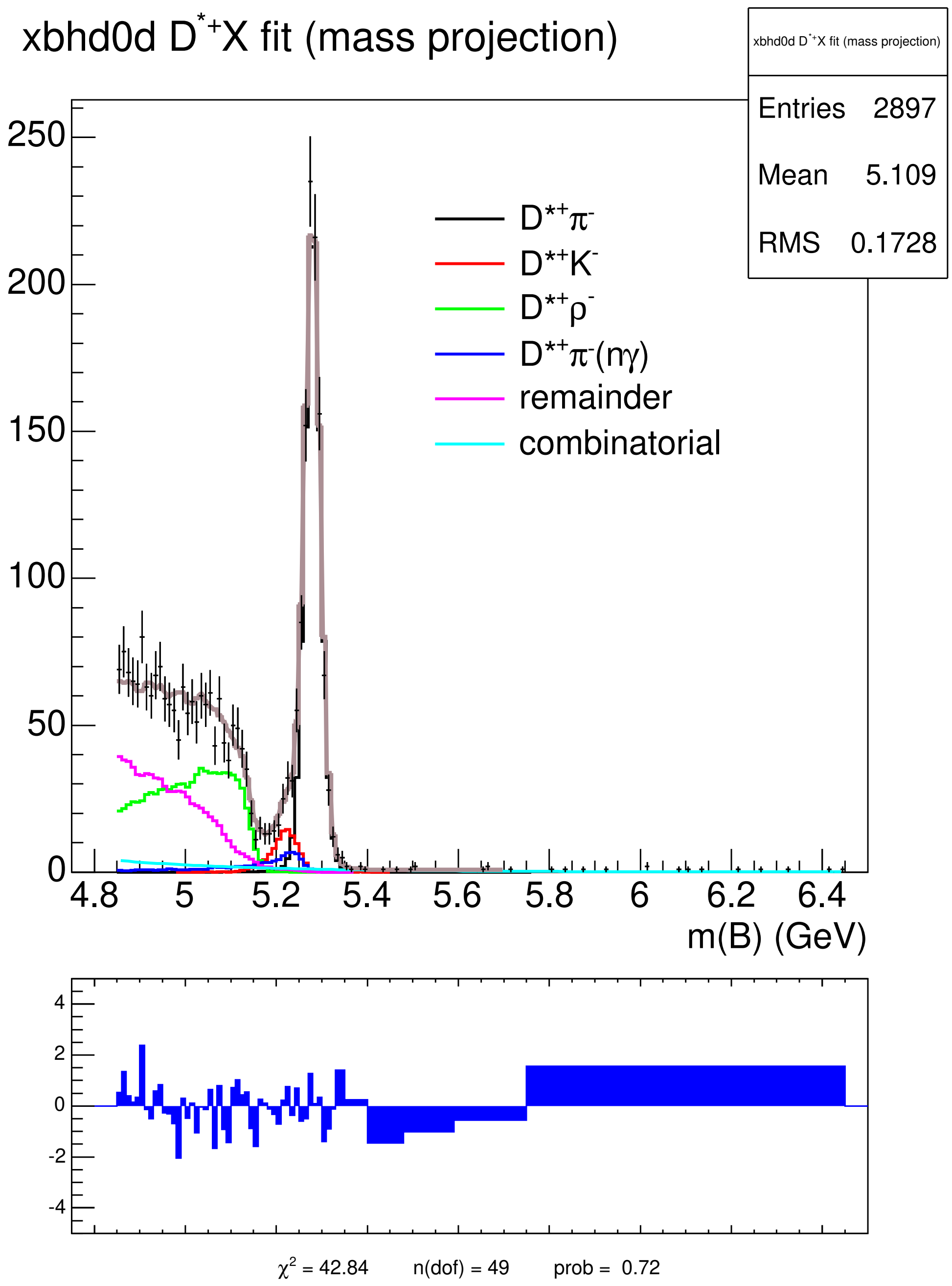

Figure 30: Mass projection of the likelihood fit results for $\overline{B}^0 \to D^{*+}\pi^-$, $D^{*+} \to D^0\pi^+$, $D^0 \to K\pi$ candidates in `xbhd0d`. The residual plot at the bottom shows the number of σ discrepancy (data minus fit). In the calculation of the residuals, neighboring bins are combined until the predicted number of events is > 5.

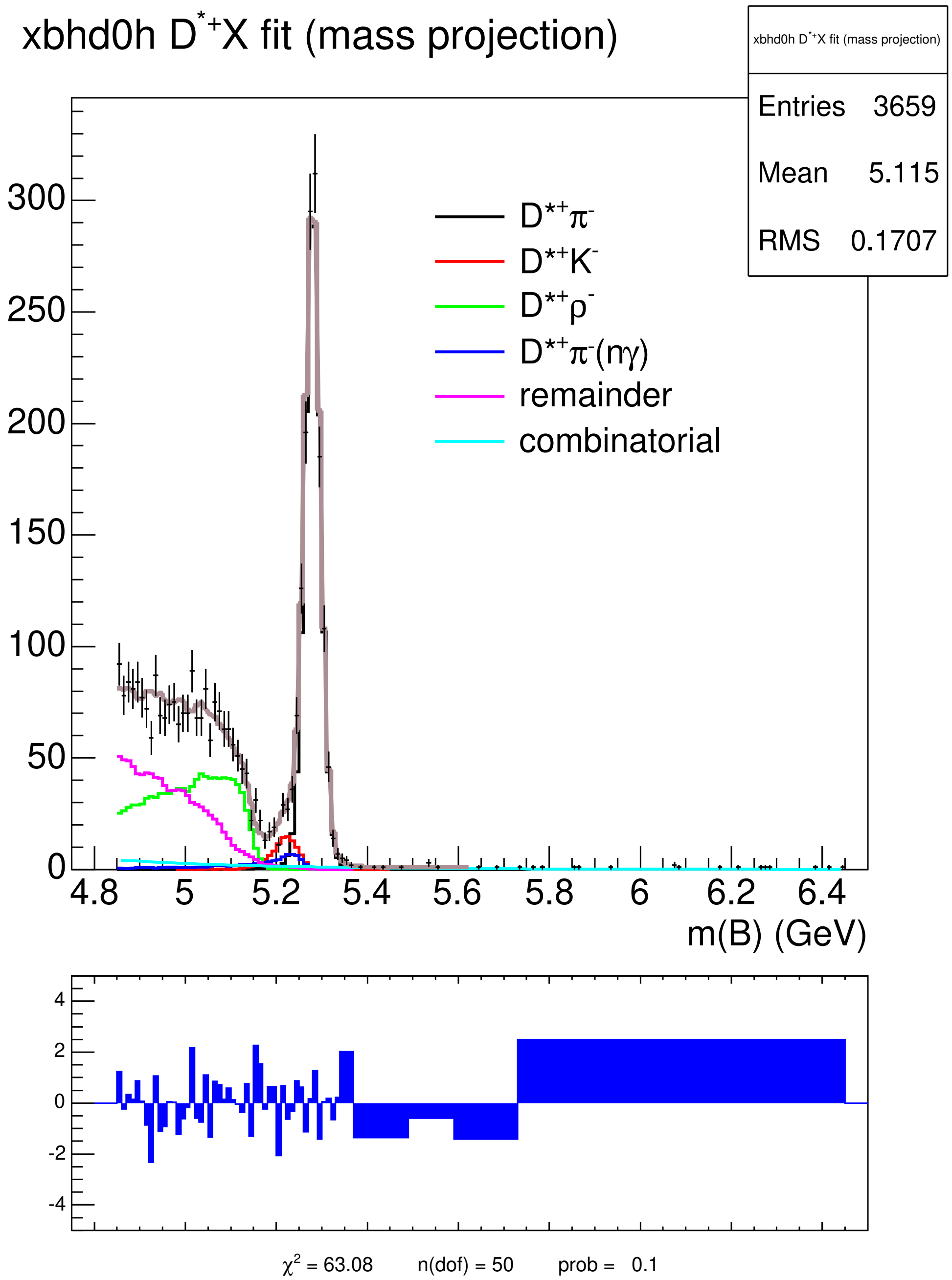

Figure 31: Mass projection of the likelihood fit results for $\overline{B}^0 \to D^{*+}\pi^-$, $D^{*+} \to D^0\pi^+$, $D^0 \to K\pi$ candidates in `xbhd0h`. The residual plot at the bottom shows the number of σ discrepancy (data minus fit). In the calculation of the residuals, neighboring bins are combined until the predicted number of events is > 5.

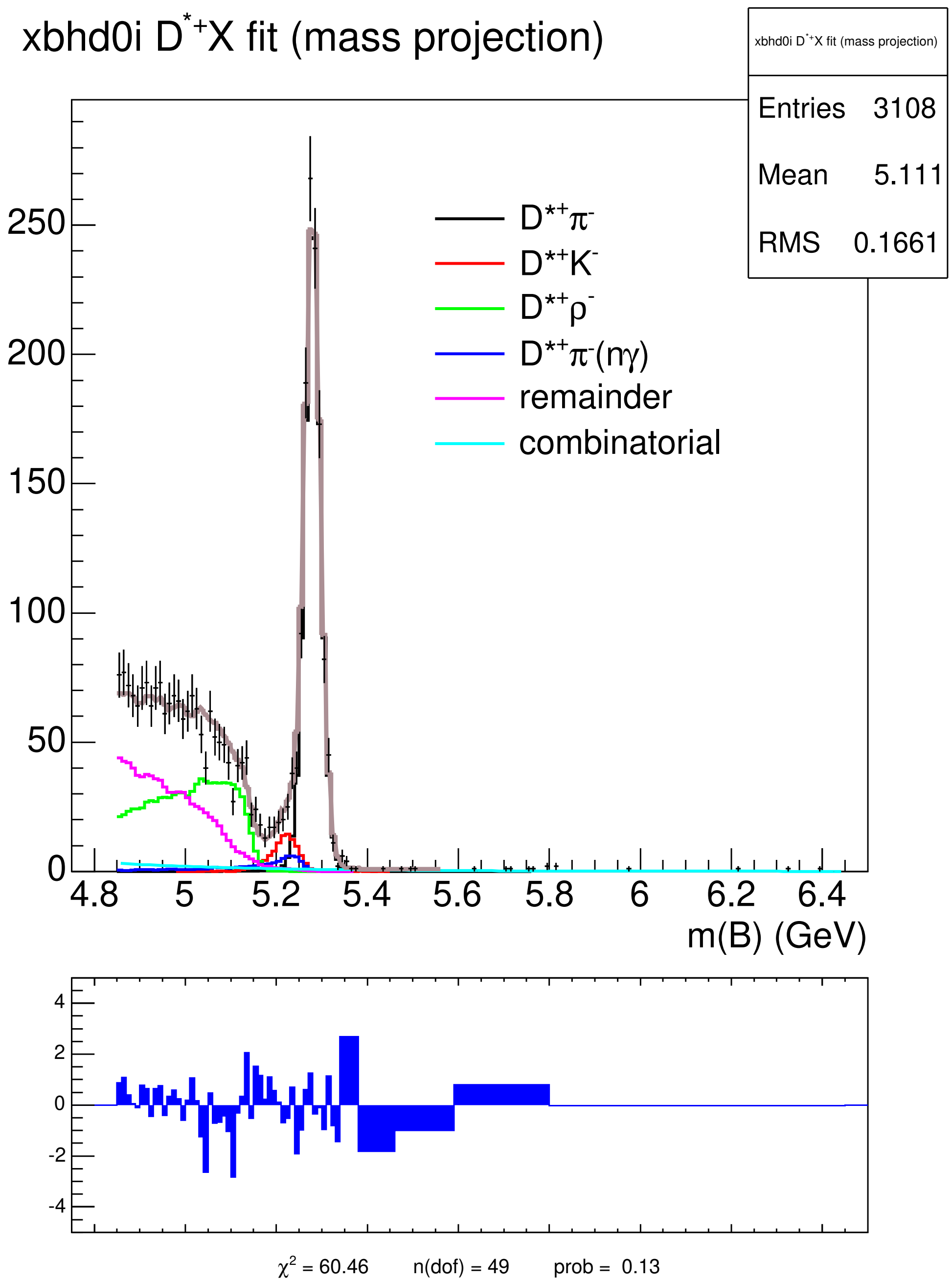

Figure 32: Mass projection of the likelihood fit results for $\overline{B}^0 \rightarrow D^{*+}\pi^-$, $D^{*+} \rightarrow D^0\pi^+$, $D^0 \rightarrow K\pi$ candidates in `xbhd0i`. The residual plot at the bottom shows the number of σ discrepancy (data minus fit). In the calculation of the residuals, neighboring bins are combined until the predicted number of events is > 5.

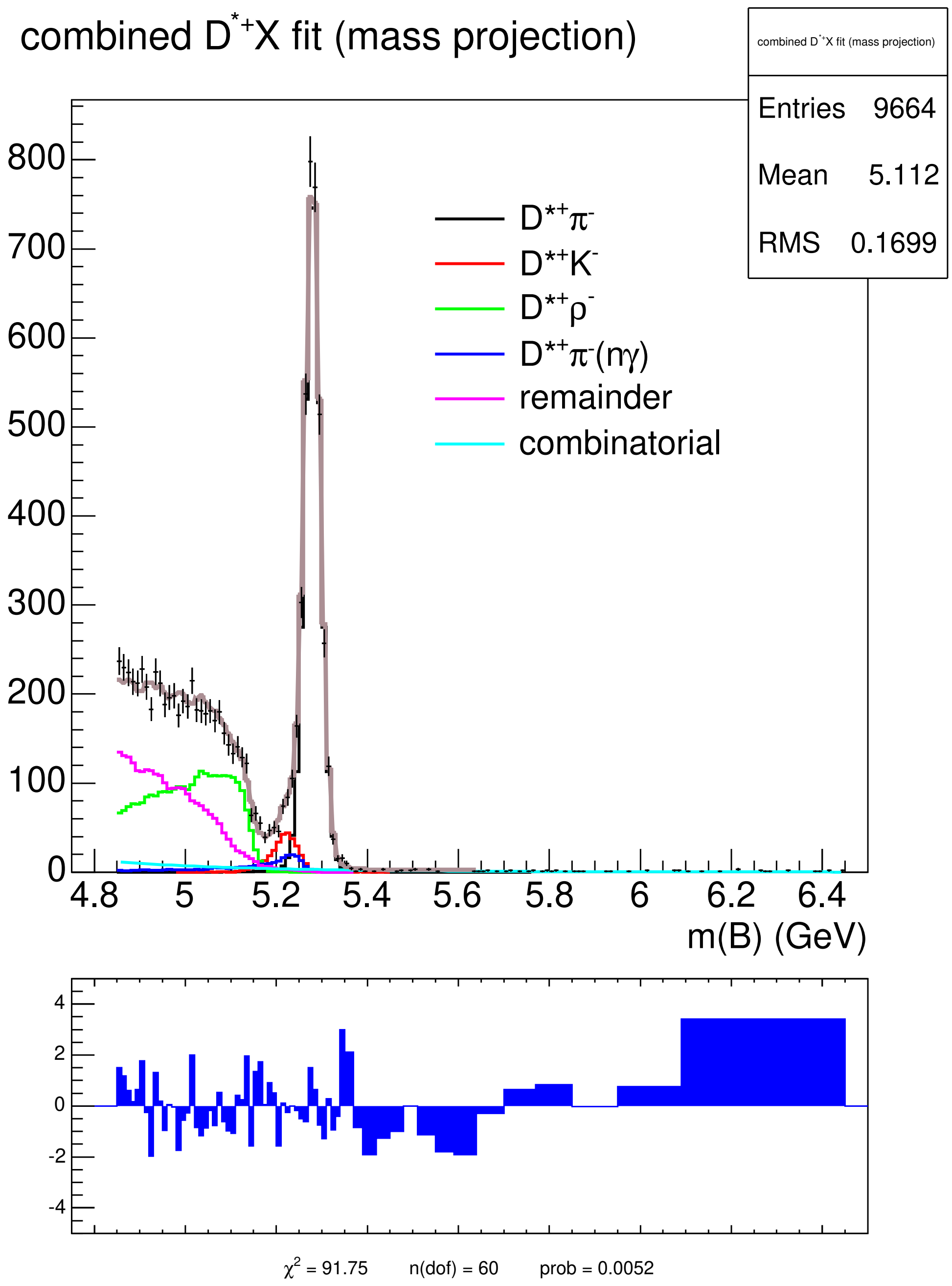

Figure 33: Mass projection of the likelihood fit results for $\overline{B}^0 \to D^{*+}\pi^-$, $D^{*+} \to D^0\pi^+$, $D^0 \to K\pi$ candidates in the combined 1.2 fb^{-1}. The residual plot at the bottom shows the number of σ discrepancy (data minus fit). In the calculation of the residuals, neighboring bins are combined until the predicted number of events is > 5.

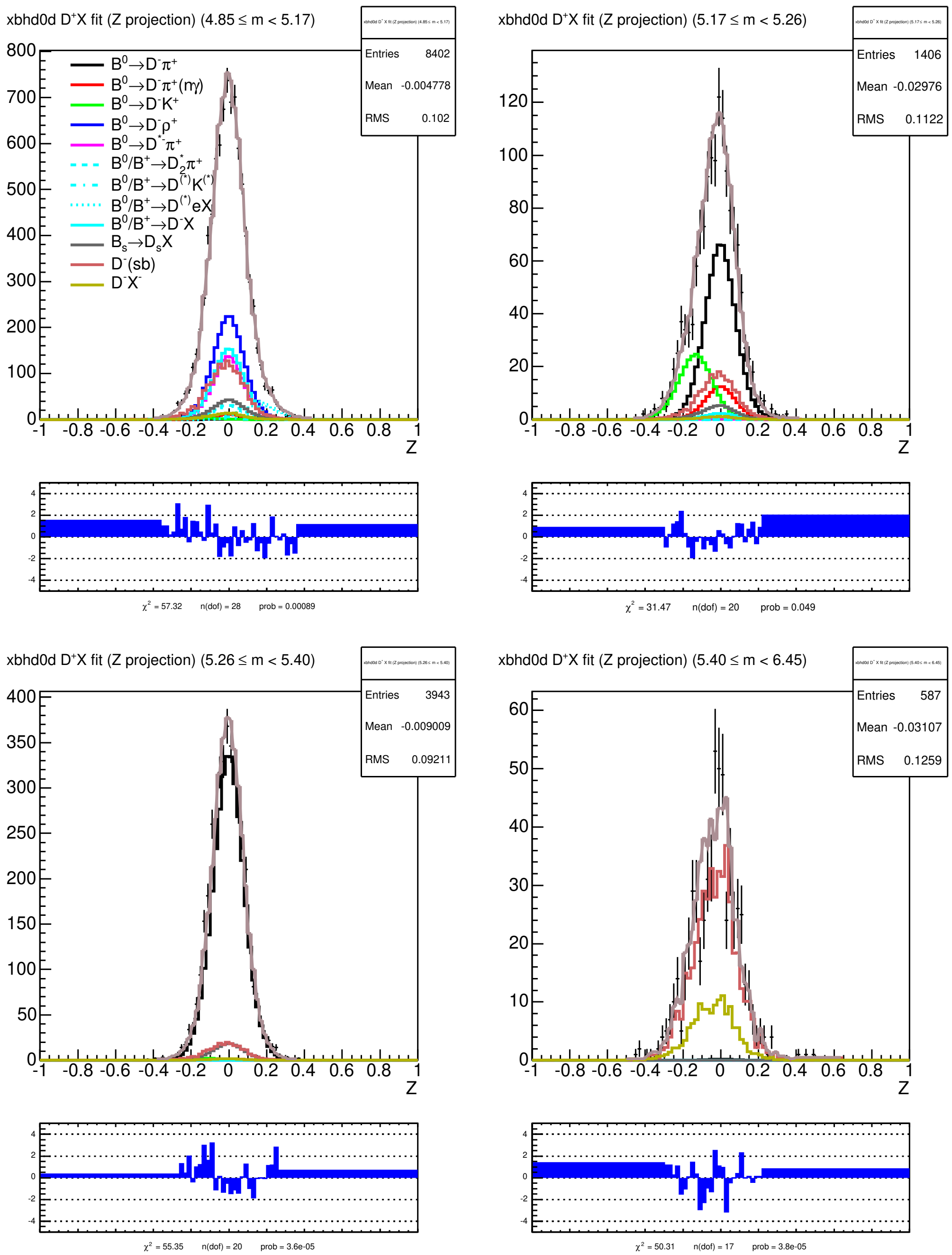

Figure 34: Z projection of the likelihood fit results for $\overline{B}^0 \to D^+\pi^-$, $D^+ \to K^-\pi^+\pi^+$ candidates in `xbhd0d`. The projections are shown in four mass regions indicated in the plot titles. The residual plot at the bottom shows the number of σ discrepancy (data minus fit). In the calculation of the residuals, neighboring bins are combined until the predicted number of events is > 5.

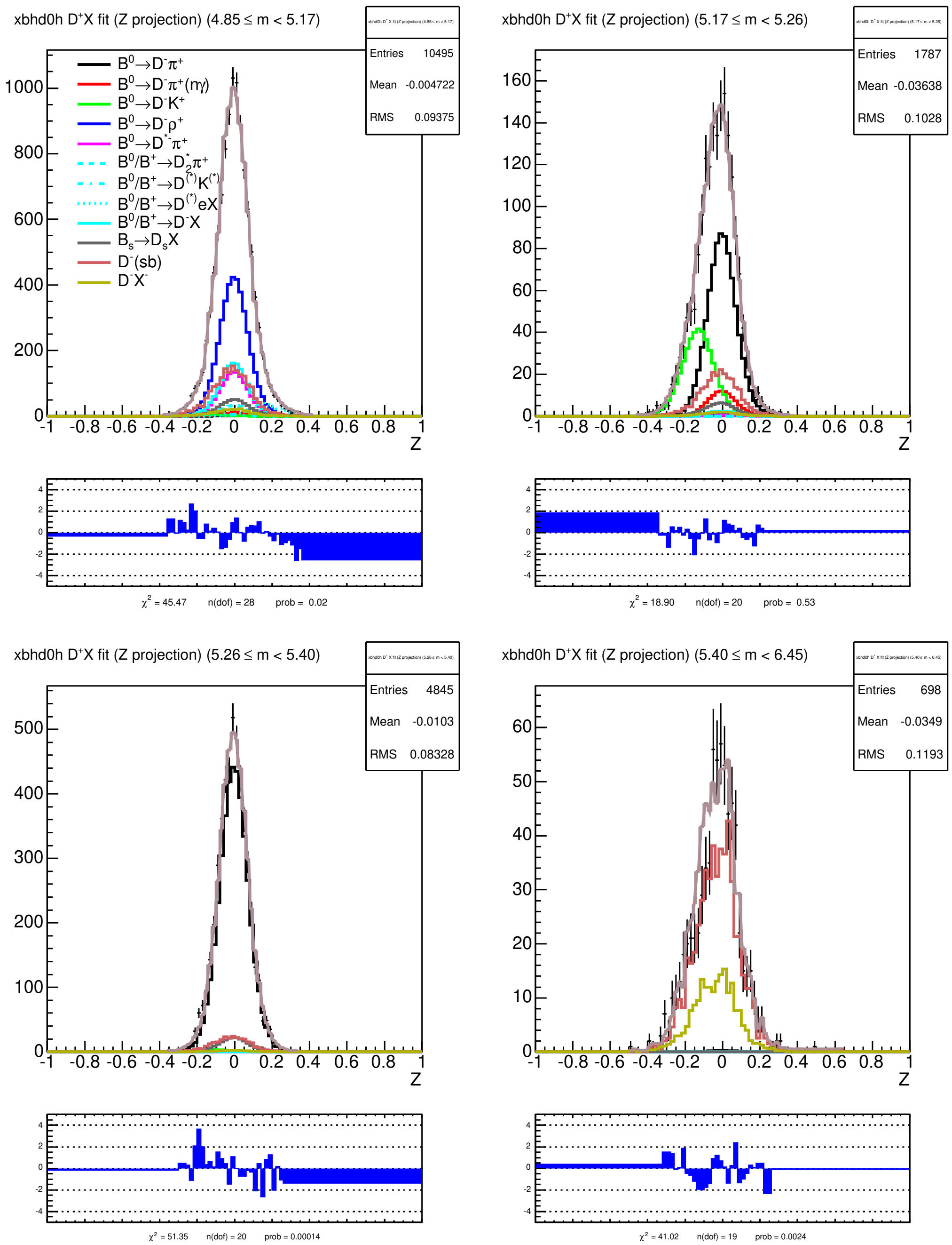

Figure 35: Z projection of the likelihood fit results for $\overline{B}^0 \to D^+\pi^-$, $D^+ \to K^-\pi^+\pi^+$ candidates in `xbhd0h`. The projections are shown in four mass regions indicated in the plot titles. The residual plot at the bottom shows the number of σ discrepancy (data minus fit). In the calculation of the residuals, neighboring bins are combined until the predicted number of events is > 5.

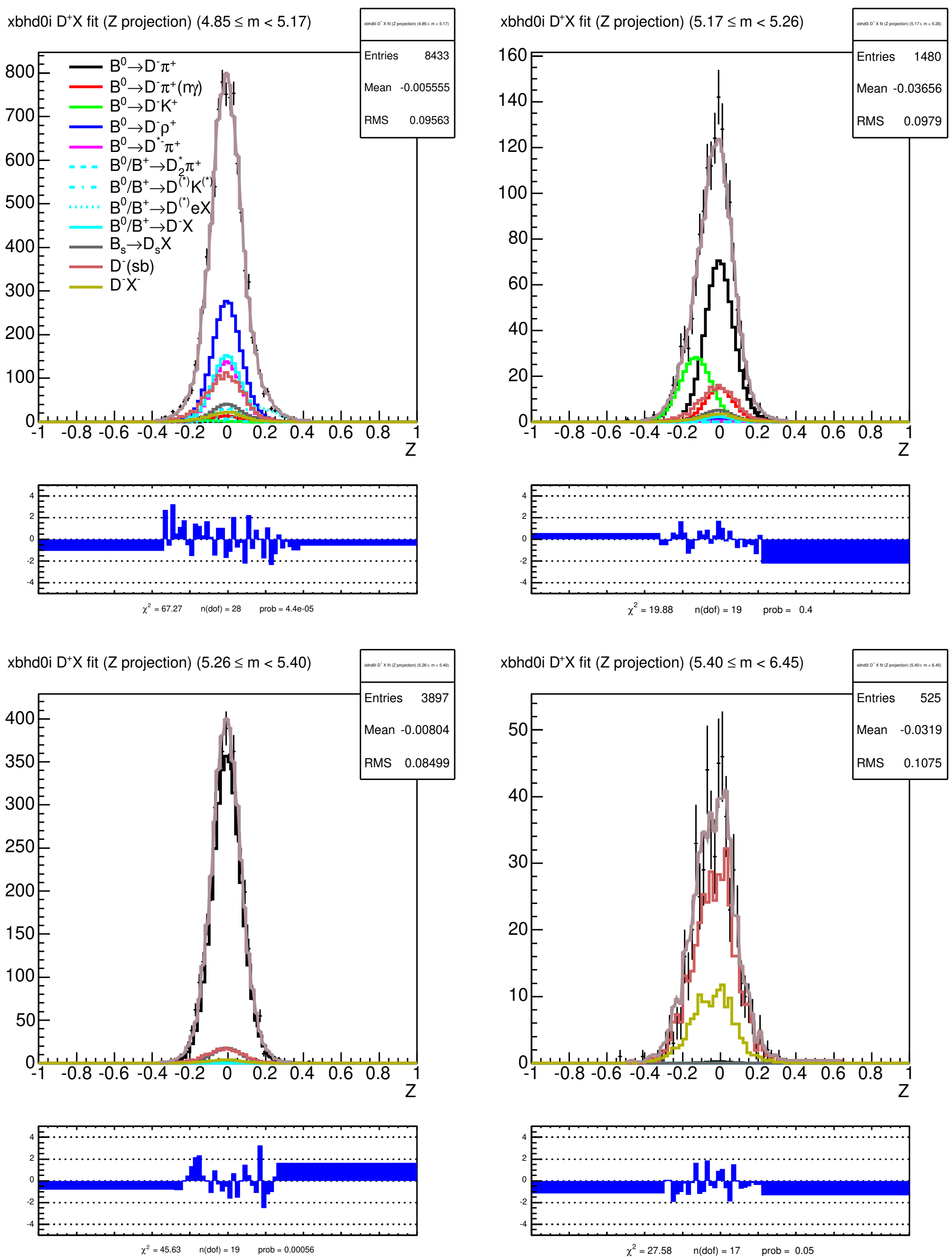

Figure 36: Z projection of the likelihood fit results for $\overline{B}^0 \to D^+\pi^-$, $D^+ \to K^-\pi^+\pi^+$ candidates in `xbhd0i`. The projections are shown in four mass regions indicated in the plot titles. The residual plot at the bottom shows the number of σ discrepancy (data minus fit). In the calculation of the residuals, neighboring bins are combined until the predicted number of events is > 5.

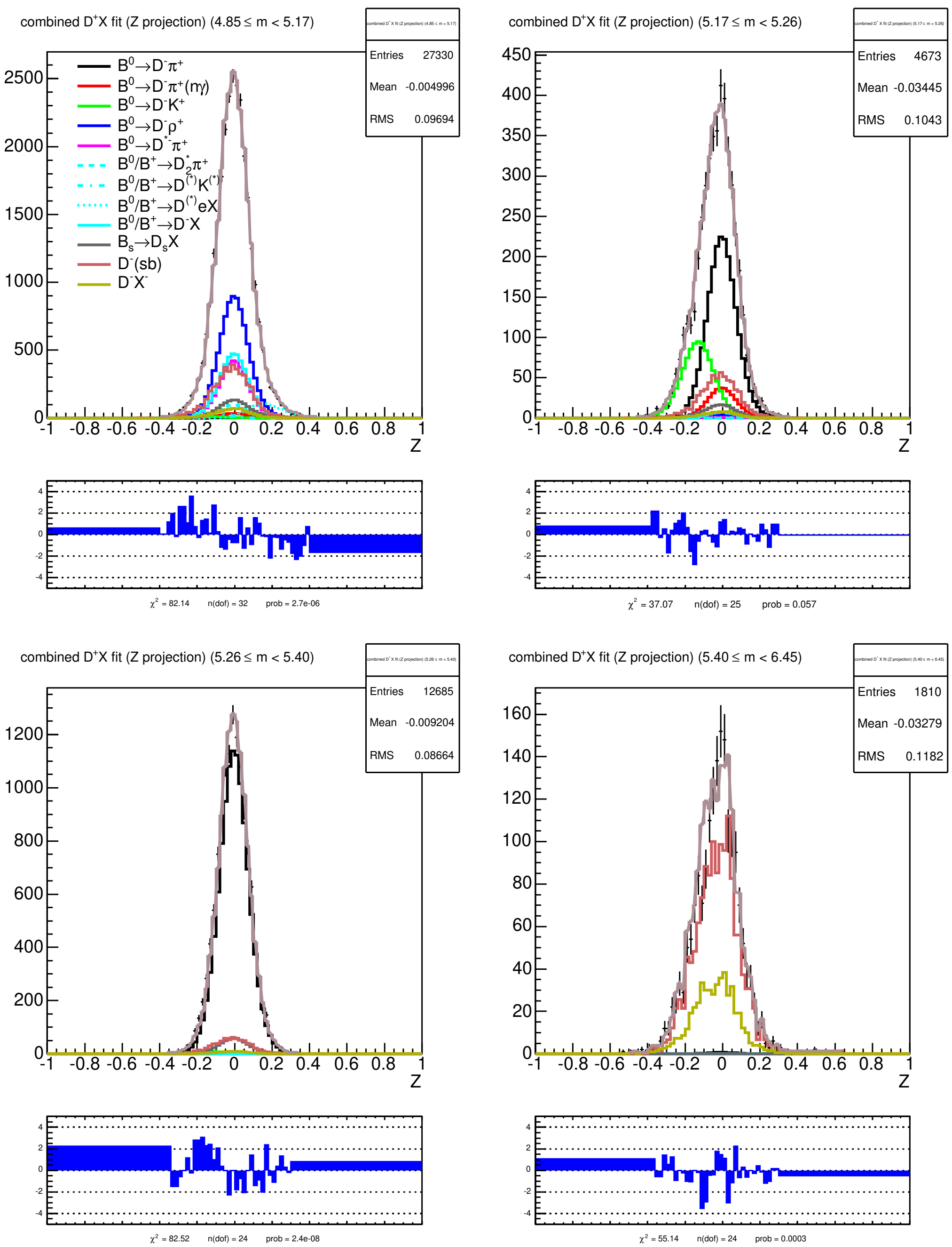

Figure 37: Z projection of the likelihood fit results for $\overline{B}^0 \to D^+\pi^-$, $D^+ \to K^-\pi^+\pi^+$ candidates in the combined 1.2 fb^{-1}. The projections are shown in four mass regions indicated in the plot titles. The residual plot at the bottom shows the number of σ discrepancy (data minus fit). In the calculation of the residuals, neighboring bins are combined until the predicted number of events is > 5.

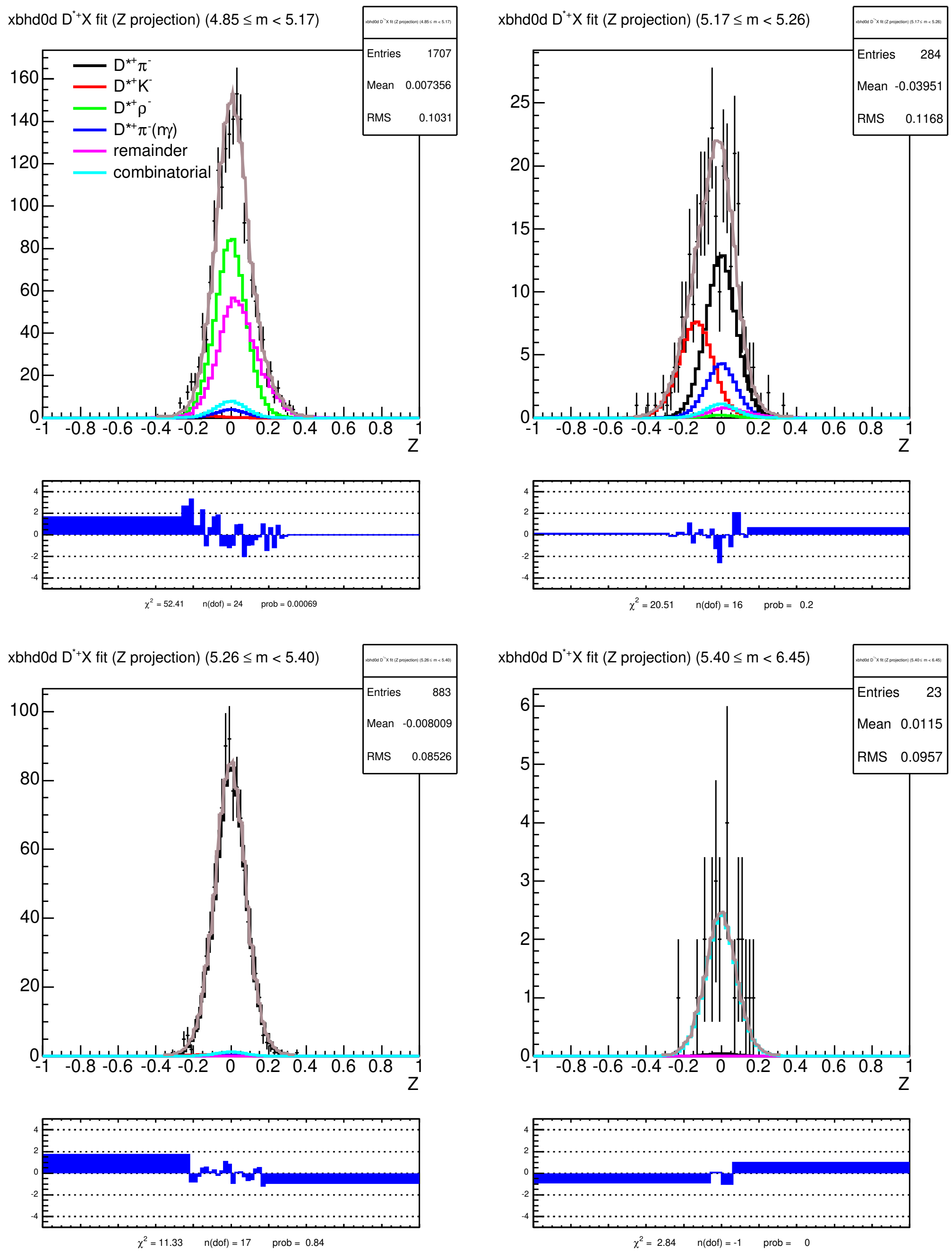

Figure 38: Z projection of the likelihood fit results for $\overline{B}^0 \to D^{*+}\pi^-$, $D^{*+} \to D^0\pi^+$, $D^0 \to K\pi$ candidates in `xbhd0d`. The projections are shown in four mass regions indicated in the plot titles. The residual plot at the bottom shows the number of σ discrepancy (data minus fit). In the calculation of the residuals, neighboring bins are combined until the predicted number of events is > 5.

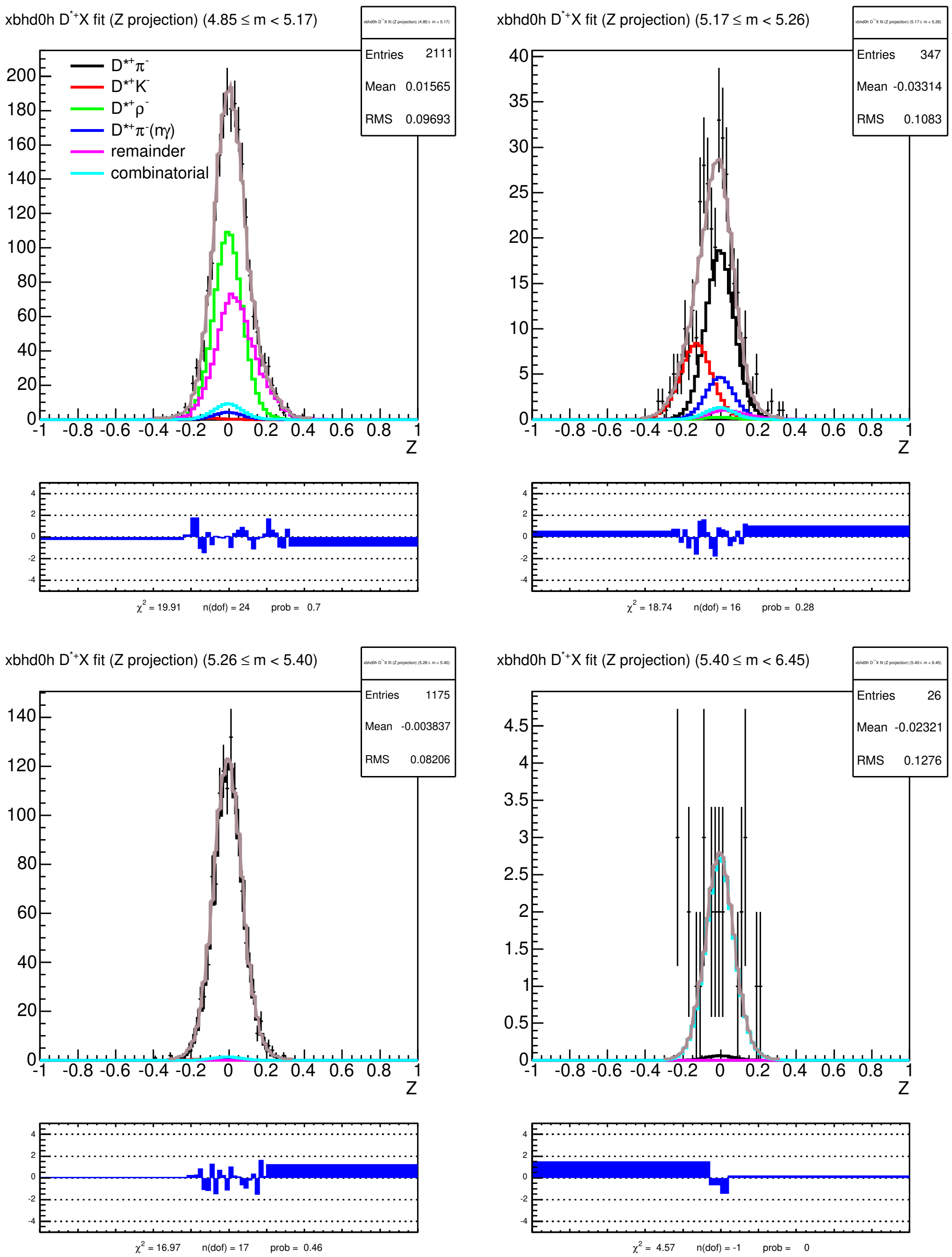

Figure 39: Z projection of the likelihood fit results for $\overline{B}^0 \to D^{*+}\pi^-$, $D^{*+} \to D^0\pi^+$, $D^0 \to K\pi$ candidates in `xbhd0h`. The projections are shown in four mass regions indicated in the plot titles. The residual plot at the bottom shows the number of σ discrepancy (data minus fit). In the calculation of the residuals, neighboring bins are combined until the predicted number of events is > 5.

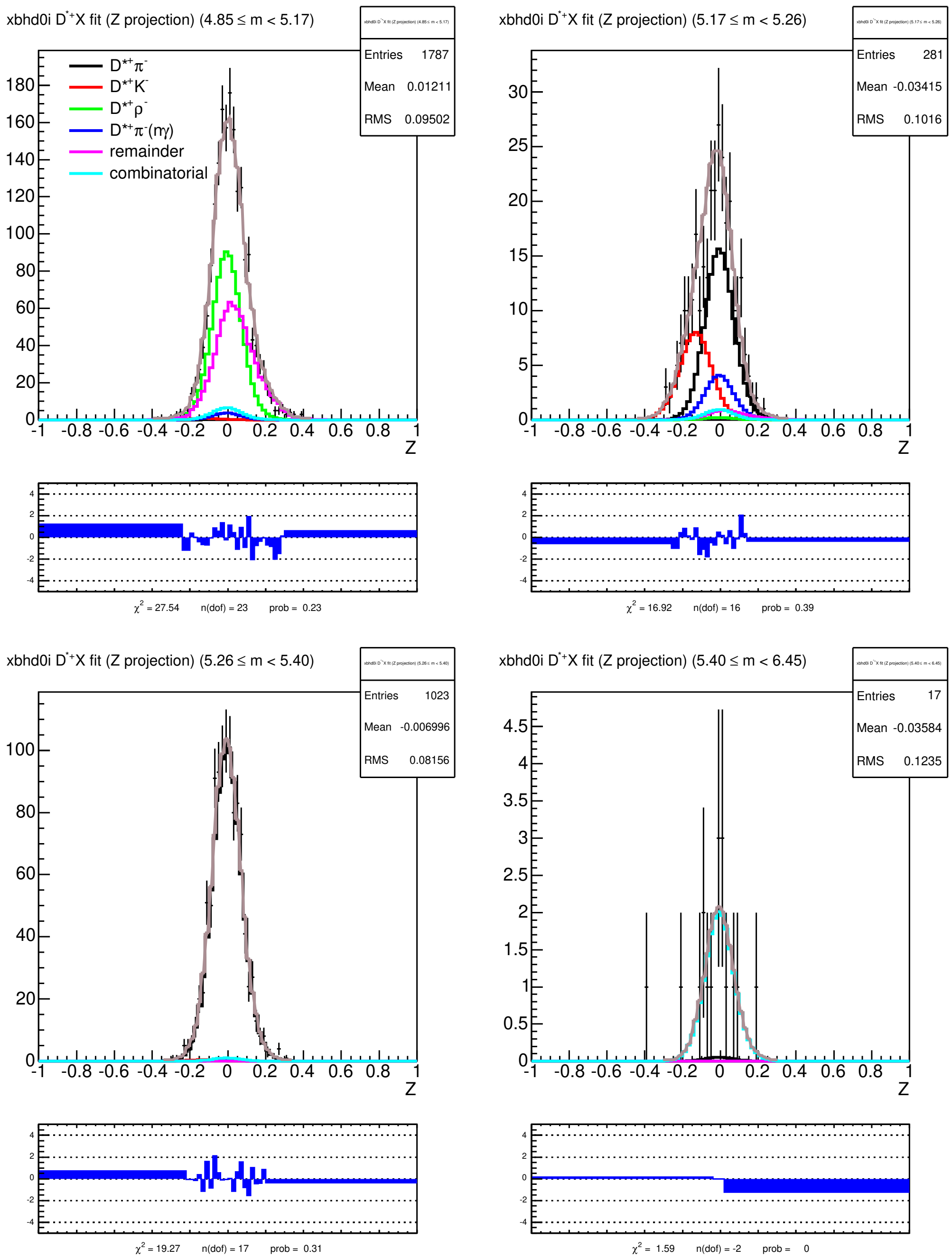

Figure 40: Z projection of the likelihood fit results for $\overline{B}^0 \to D^{*+}\pi^-$, $D^{*+} \to D^0\pi^+$, $D^0 \to K\pi$ candidates in `xbhd0i`. The projections are shown in four mass regions indicated in the plot titles. The residual plot at the bottom shows the number of σ discrepancy (data minus fit). In the calculation of the residuals, neighboring bins are combined until the predicted number of events is > 5.

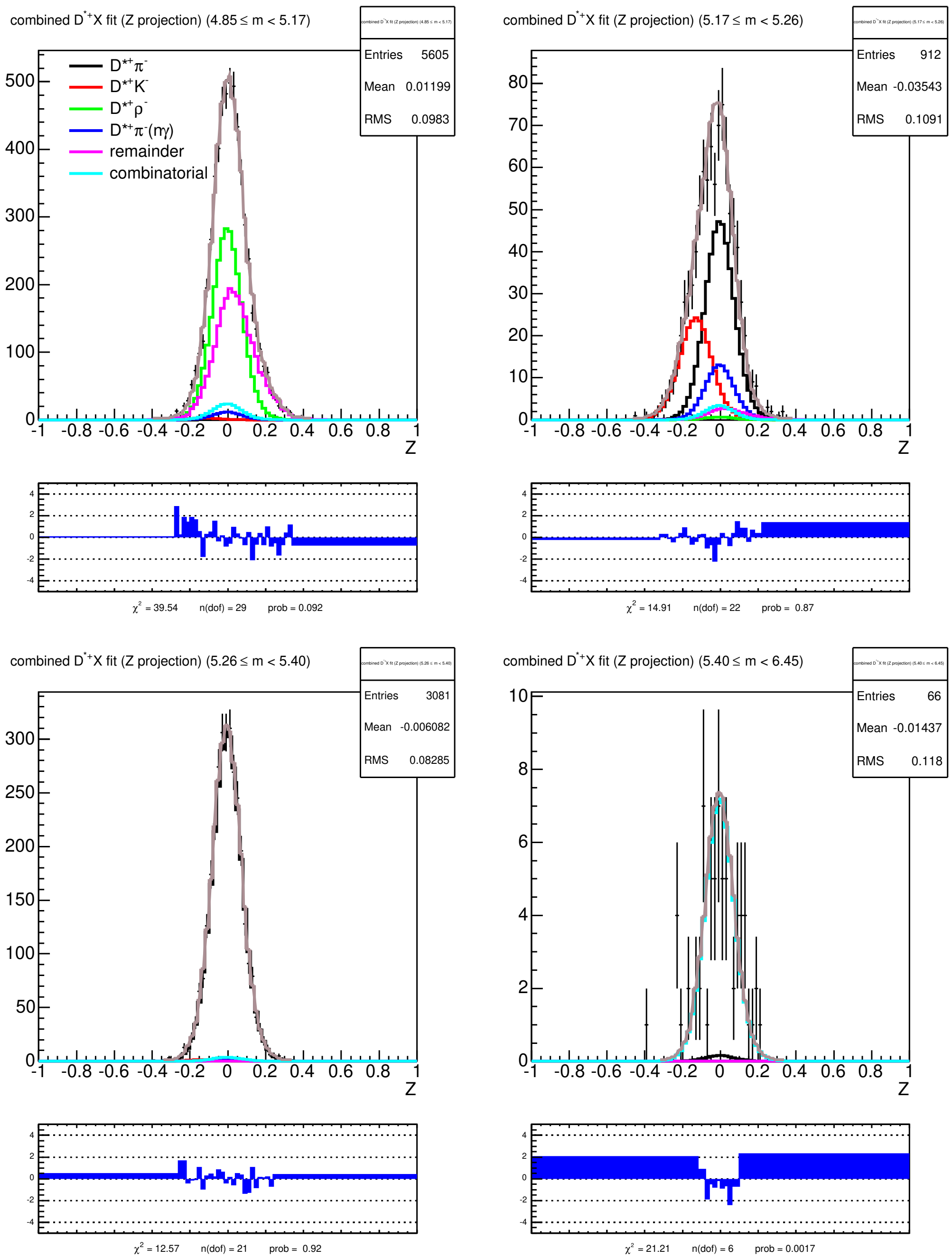

Figure 41: Z projection of the likelihood fit results for $\overline{B}^0 \rightarrow D^{*+}\pi^-$, $D^{*+} \rightarrow D^0\pi^+$, $D^0 \rightarrow K\pi$ candidates in the combined 1.2 fb^{-1}. The projections are shown in four mass regions indicated in the plot titles. The residual plot at the bottom shows the number of σ discrepancy (data minus fit). In the calculation of the residuals, neighboring bins are combined until the predicted number of events is > 5.

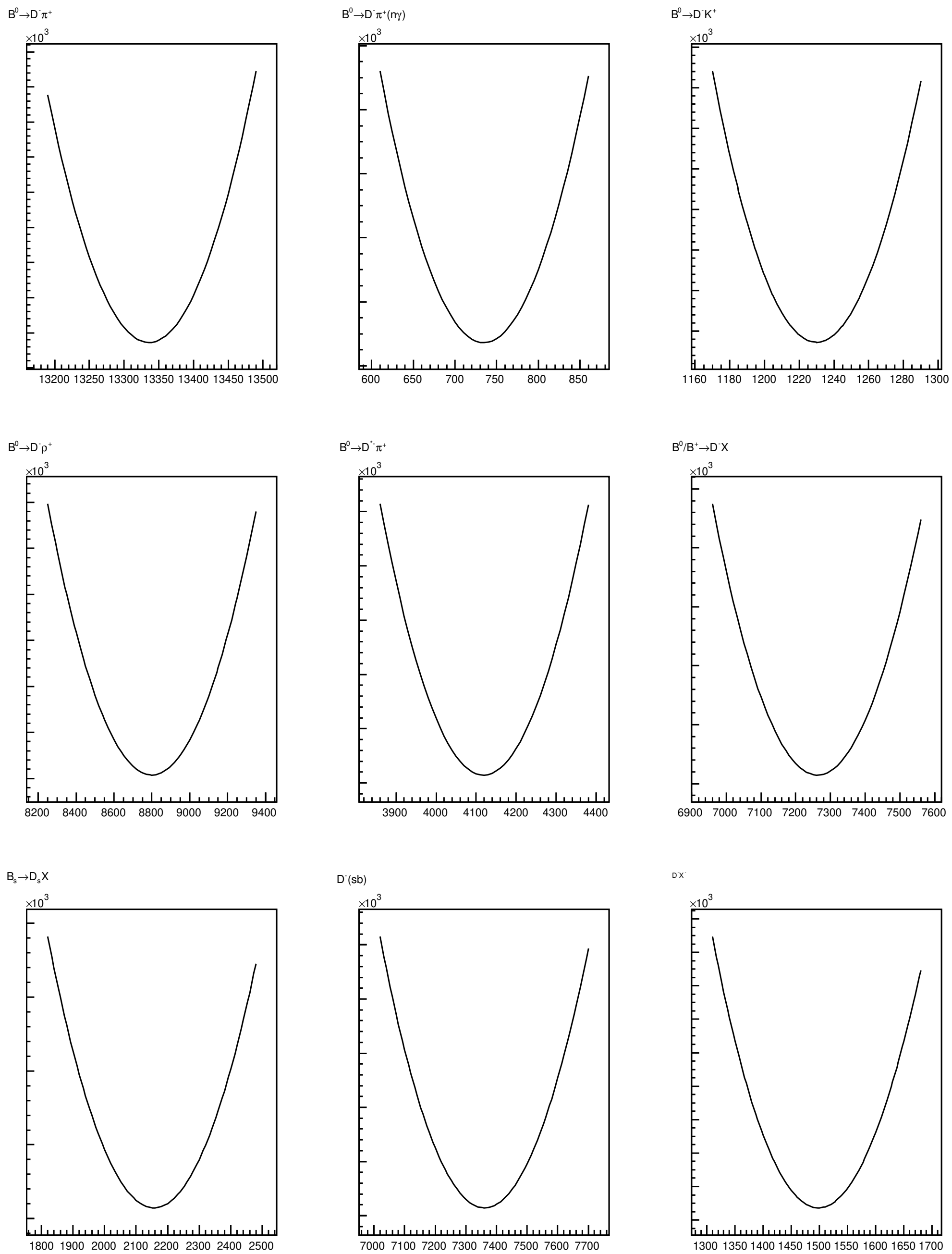

Figure 42: Likelihood scans for $\overline{B}^0 \to D^+ \pi^-$

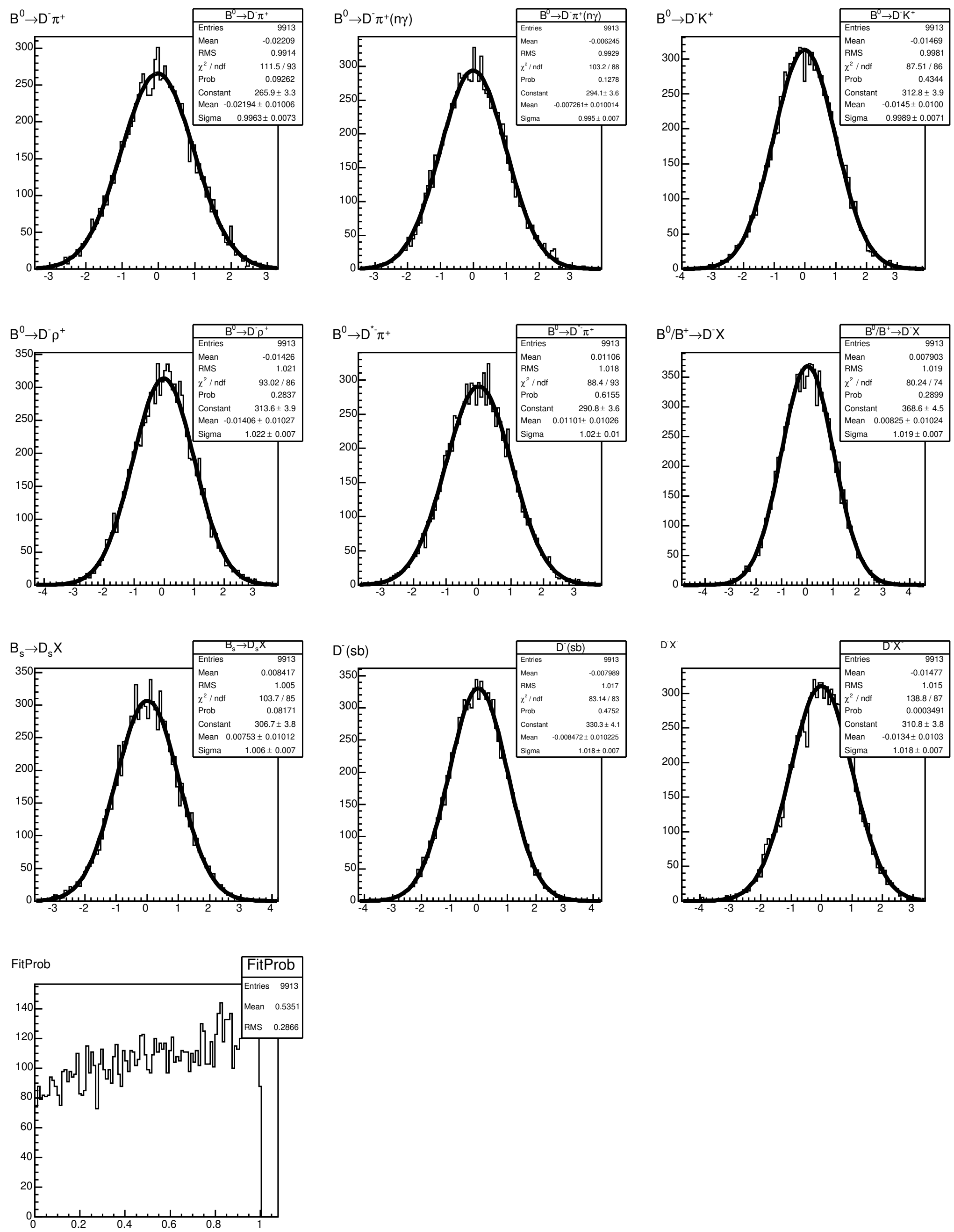

Figure 43: Pull distributions for $\overline{B}^0 \to D^+\pi^-$

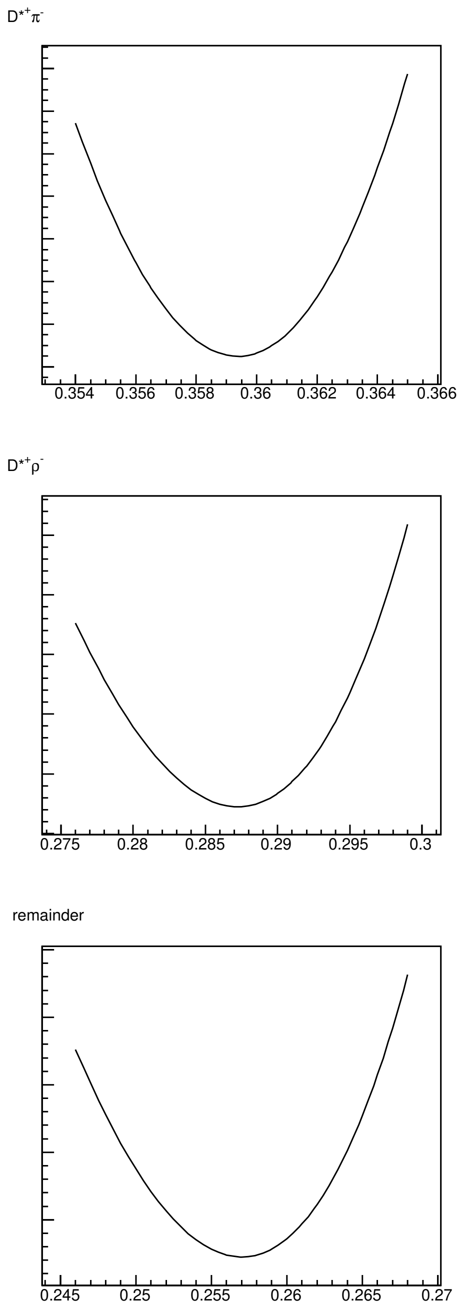

Figure 44: Likelihood scans for $\overline{B}^0 \to D^{*+}\pi^-$

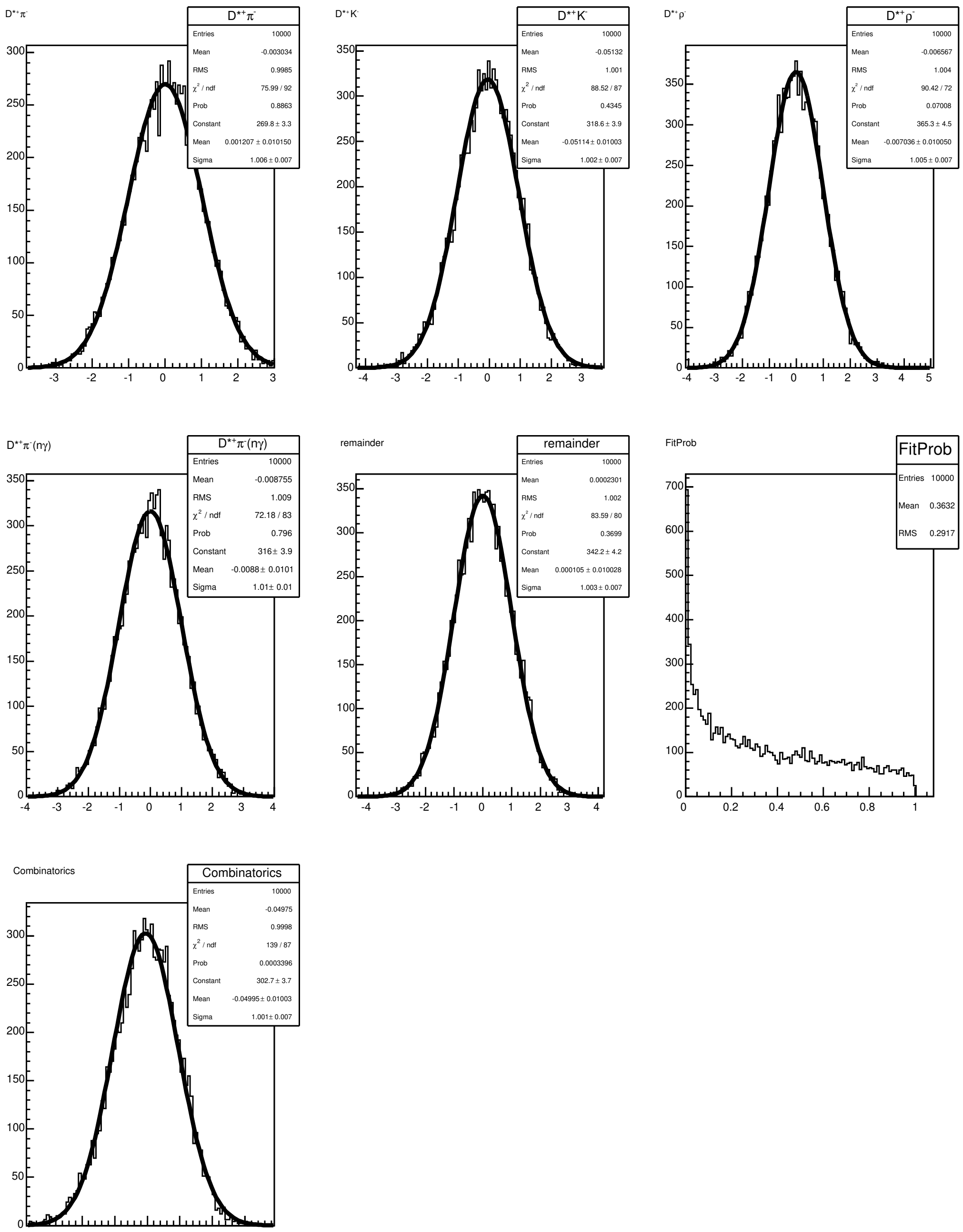

Figure 45: Pull distributions for $\overline{B}^0 \to D^{*+}\pi^-$

References

[1] M. Gronau and D. London., Phys. Lett. **B253**, 483 (1991).

[2] M. Gronau and D. Wyler, Phys. Lett. **B265**, 172 (1991).

[3] M. Gronau, Phys. Rev. **D58**, 037301 (1998), hep-ph/9802315.

[4] D. Atwood, I. Dunietz and A. Soni, Phys. Rev. **D63**, 036005 (2001), hep-ph/0008090.

[5] A. Giri, Y. Grossman, A. Soffer and J. Zupan, Phys. Rev. **D68**, 054018 (2003), hep-ph/0303187.

[6] R. Aleksan, I. Dunietz and B. Kayser, Z. Phys. **C54**, 653 (1992).

[7] A. Cerri, A. Deisher, H.-C. Fang, J. Mülmenstädt and M.D. Shapiro, Measurement of B^+ branching fractions using a combined mass and dE/dx fit, CDF note 8777.

[8] A. Cerri, A. Deisher, H.-C. Fang, J. Mülmenstädt and M.D. Shapiro, Measurement of B_s^0 branching fractions using a combined mass and dE/dx fit, CDF note 8776.

[9] B_s mixing group, Updated measurement of Δm_d and calibration of flavor tagging in fully reconstructed decays, CDF note 7722.

[10] S. Giagu *et al.*, `http://www-cdf.fnal.gov/internal/physics/bottom/bpak/pid/COT-_Dedx_V11_root4.C`.

[11] `http://www-cdf.fnal.gov/htbin/twiki/bin/view/JohnsHopkins/BtoDXMonte-CarloGeneration`.

[12] A. Cerri, A. Deisher, H.-C. Fang, J. Mülmenstädt and M.D. Shapiro, dE/dx templates for the measurement of the relative branching ratios $\mathcal{B}(B \to DK) \,/\, \mathcal{B}(B \to D\pi)$, CDF note 8716.

[13] S. Giagu *et al.*, Track-based calibration of the COT specific ionization, CDF note 6932.

[14] K. Abe *et al.*, Phys. Rev. **D69**, 112002 (2004), hep-ex/0307021.

[15] S. Giagu *et al.*, BR ratios and direct *CP* violation in Cabibbo suppressed decays of D^0, CDF note 6391.

[16] K. Abe *et al.*, Phys. Rev. Lett. **87**, 111801 (2001), hep-ex/0104051.

[17] B. Aubert *et al.*, Phys. Rev. Lett. **96**, 011803 (2006), hep-ex/0509036.